[AMERICAN JOURNAL OF SCIENCE, VOL. 296, MAY, 1996, P. 506–548]

A THERMODYNAMIC MODEL FOR WATER COLUMN PRECIPITATION OF SIDERITE IN THE PLIO-PLEISTOCENE BLACK SEA

S. RAJAN*, FRED T. MACKENZIE**, and CRAIG R. GLENN*

ABSTRACT. It has been hypothesized that finely disseminated, soft, wheat-like grains of siderite in the sideritic muds of the Plio-Pleistocene section of the Black Sea are "sub-aqueous precipitates" (Hsü and Kelts, 1978). In an attempt to quantify this hypothesis, we (1) investigated the chemistry, mineralogy, and isotopic composition of the siderites and associated calcite and (2) developed a thermodynamic model of endogenic siderite precipitation (that is, directly precipitated from the water column) driven by sequential evaporative concentration of acidic, dissolved organic-carbon, and iron-rich waters. Considering the average composition of the present-day Satilla drainage of the southeastern United States as approximating the composition of the waters that fed the Neogene Black Sea and allowing this water to evaporate isothermally at 25°C in equilibrium with atmospheric CO_2 ($PCO_2 = 10^{-3.5}$ atm), we calculated the aqueous concentrations at which various carbonate phases would precipitate out of the system. It is shown that evaporation of this water to roughly one-twelfth of its original volume can result in precipitation of the pure endmember siderite alone. Relating our geochemical and modeling results to the details of Black Sea climatostratigraphic and evolutionary history during the times of deposition of the siderite units, we corroborate the qualitative arguments of Hsü and Kelts (1978). We also conclude that climate was the chief forcing function in transforming episodically the calcite-precipitating eutrophic water masses of the Plio-Pleistocene basin to one of siderite precipitation. Based on our model calculations of the thickness of siderite precipitated per cm^2 of basin area, we further predict that the observed laminae/interbeds of siderite could be a composite of several microlayers of siderite and clays.

INTRODUCTION

Siderite ($FeCO_3$) is the most common authigenic carbonate in iron-bearing sediments of all ages (James, 1966; Maynard, 1983). Concentrations and cemented layers of this mineral, attributed to early diagenetic precipitation from interstitial waters or at the sediment-water interface, have been reported from a variety of ancient and modern settings, from shallow marine to coastal, floodplain, deltaic, and fresh water lacustrine environments (Curtis, 1967; Fritz and others, 1971; Postma, 1977, 1981, 1982; Matsumoto and Iijima, 1981; Gautier, 1982; Bahrig, 1988, 1989; Glenn and Arthur, 1990; Pye and others, 1990; Mozley and Carothers, 1992; Moore, Ferrell, and Aharon, 1992; Spiro, Gibson, and Shaw, 1993). The geochemical controls on the formation and distribution of these diagenetic precipitates are fairly well documented. In general, siderite

* Department of Geology and Geophysics, SOEST, University of Hawaii, 2525 Correa Road, Honolulu, Hawaii 96822.

** Department of Oceanography, SOEST, University of Hawaii, 1000 Pope Road, Honolulu, Hawaii 96822.

has a very limited thermodynamic field of stability (fig. 1), and its occurrence in sediments necessitates rather restricted environmental conditions of low pe and high PCO_2. Availability of organic matter, HCO_3^- activity or total CO_2 concentration, low dissolved sulfide concentration, and microbial activity all influence the origin of siderite and its subsequent diagenetic alteration (Curtis and Spears, 1968). As shown in figure 1, even at a total CO_2 concentration of 10^{-3} moles l^{-1} and a concentration of dissolved sulfur species of 10^{-8} moles l^{-1}, the stability

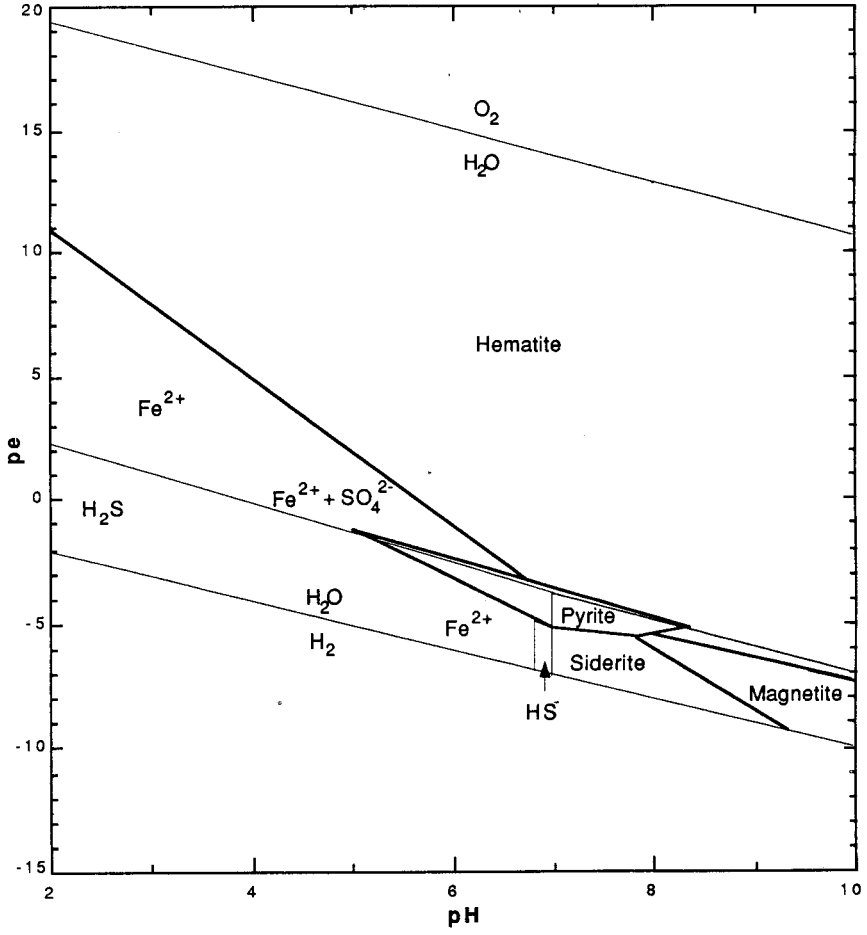

Fig. 1. pE-pH diagram showing the calculated stability fields of iron, siderite, and other iron-species in H_2O at 25°C and 1 atm total pressure, assuming $a_{Fe^{2+}} = 10^{-6}$, $\Sigma S = 10^{-8}$, $\Sigma CO_2 = 10^{-3.0}$ moles l^{-1}. Free energy values used are from Burton, Machel, and Qi (1993), Helgeson and others (1978), Robie, Hemingway, and Fisher (1979), Shock and Helgeson (1988), and Tardy and Garrels (1976).

field of siderite is very small. Under these conditions, with increasing sulfide concentration, any ferrous iron might be expected to be precipitated as sulfide (greigite, mackinawite, or pyrite), rather than as the carbonate phase.

Three distinct geochemical environments have been demonstrated to be conducive to siderite precipitation during early diagenesis. In slowly deposited pelagic sediments with relatively low concentrations of organic matter, vertically expanded depth zones of iron reduction (that is, suboxic diagenesis, Froelich and others, 1979; Berner, 1981; Maynard, 1982) constitute an ideal environment for siderite precipitation (Curtis, 1977; Walker, 1984; Coleman, 1985; Mozley and Carothers, 1992). Siderite precipitation is also highly favored in the zone of methanogenesis, especially if the sediments are not iron-limited. However, conditions for siderite formation beneath anoxic marine waters in the sulfate reduction zone of sediments are more complex than in the zones of iron reduction or methanogenesis (Curtis, 1987). Iron-rich carbonates can coprecipitate with iron sulfides only if sufficient reactive iron is available and the rate of iron reduction balances or exceeds that of sulfate reduction (Curtis, 1987; Pye and others, 1990). Because continental lacustrine settings are characterized by low dissolved sulfate and consequently sufide concentrations, high rates of sedimentation and relatively high organic carbon flux, these settings are the most ideally suited environments with respect to siderite precipitation during early diagenesis.

Endogenic (inorganic, water-column derived) siderites appear to be uncommon in the ancient sediment record. This is a rather intriguing observation because the conditions stipulated for siderite formation and thermodynamic stability (low pe, low dissolved sulfide concentrations, availability of reactive iron, and high PCO_2) can also be attained in the bottom waters of a depositional basin, in addition to the pore water realm. Klein and Beukes (1989), Beukes and others (1990), and Beukes and Klein (1992), based on petrographic and geochemical studies of the iron-formation sequences in the Transvaal Supergroup of South Africa, established that most of the siderite forming finely laminated units is a primary sedimentary precipitate from the water column or at the sediment-water interface. Similarly, the fine-scale alteration of iron-rich and iron-poor microbands in the iron-formations of the Hamersley Range, Western Australia, has been interpreted as the result of deep water deposition linked with evaporation (Trendall and Blockley, 1970). Garrels (1987, 1988) demonstrated that the Hamersley Range microbands could also result from evaporation of stream waters in a non-marine basin. In modern lacustrine settings, however, precipitation of siderite from the water column has been shown to occur only in the Cameroon volcanic lakes of Monoun and Nyes (Sigurdsson and others, 1987; Bernard and Symonds, 1989). According to the model developed by these authors to explain the lethal gas burst episodes from these lakes, steady-state input of CO_2 from cold volcanic vents within these lake basins

over an extended period of time led to the build-up of dissolved bicarbonate. Reduction by reaction with organic matter, of laterite-derived ferric hydroxides reaching the stagnant, anoxic hypolimnion of the lake basin, led to high hypolimnion concentration of Fe^{2+}. Catastrophic CO_2-gas burst episodes and resultant degassing in these lakes apparently increased saturation with respect to siderite leading to its precipitation (Sigurdsson and others, 1987; Bernard and Symonds, 1989).

Hsü and Kelts (1978), in studies of chemical sedimentation in the Black Sea, suggested for the first time the probability that the spindle-shaped siderite grains in the Neogene muds of the basin could be precipitates from the water column (endogenic). According to them, the persistence of a warm, humid climate during the times of siderite deposition led to intense chemical weathering of hinterland lithologies, yielding abundant fluvial inputs of iron and silica to a fresh water Black Sea basin. The deeper waters of this basin must have been periodically anoxic as a consequence of biological productivity, to allow for remobilization of iron and manganese as Fe^{2+} and Mn^{2+}. Hsü and Kelts further suggested that the water chemistry of the Neogene drainage into the Black Sea was similar to that of the sluggish streams of the southeastern United States, which are characterized by a relatively high content of dissolved organic matter, iron and silica, and low concentrations of other dissolved ions such as Ca^{2+} and Mg^{2+}. Availability of reactive iron and low sulfide concentrations in an eutrophic water mass with anoxic basinal conditions might have led to an increase in saturation conditions favoring siderite precipitation.

The purpose of this paper is to test and expand on the Hsü-Kelts hypothesis and to develop a thermodynamic model of primary siderite precipitation in a fresh water environment driven by sequential evaporative concentration of acidic, dissolved organic-carbon and iron-rich waters in a basin with a net hydrographic deficit. The basic features of the model closely follow the evaporative concentration model of Sierra Springs developed by Garrels and Mackenzie (1967), as well as a thermodynamic evaporative model for the microbanded Precambrian Iron Formations suggested by Garrels (1987). As suggested by Hsü and Kelts (1978), we elected to use the composition of one of the present-day rivers draining southern Georgia, U.S.A. (the Satilla River), as approximating the composition of the feedwaters draining into the Neogene Black Sea. The silt-sized grains of siderite in the two siderite-bearing units of the Black Sea (fig. 2) are considered to be the ultimate end products of such deposition. The paleo-environmental conditions and the history of chemical carbonate sedimentation in the basin during Plio-Pleistocene times provide further constraints on the model. Our theoretical development is therefore preceded by a brief discussion of these constraints and the considerations that are necessary in relating the model results to the hypothesis of endogenic siderite precipitation.

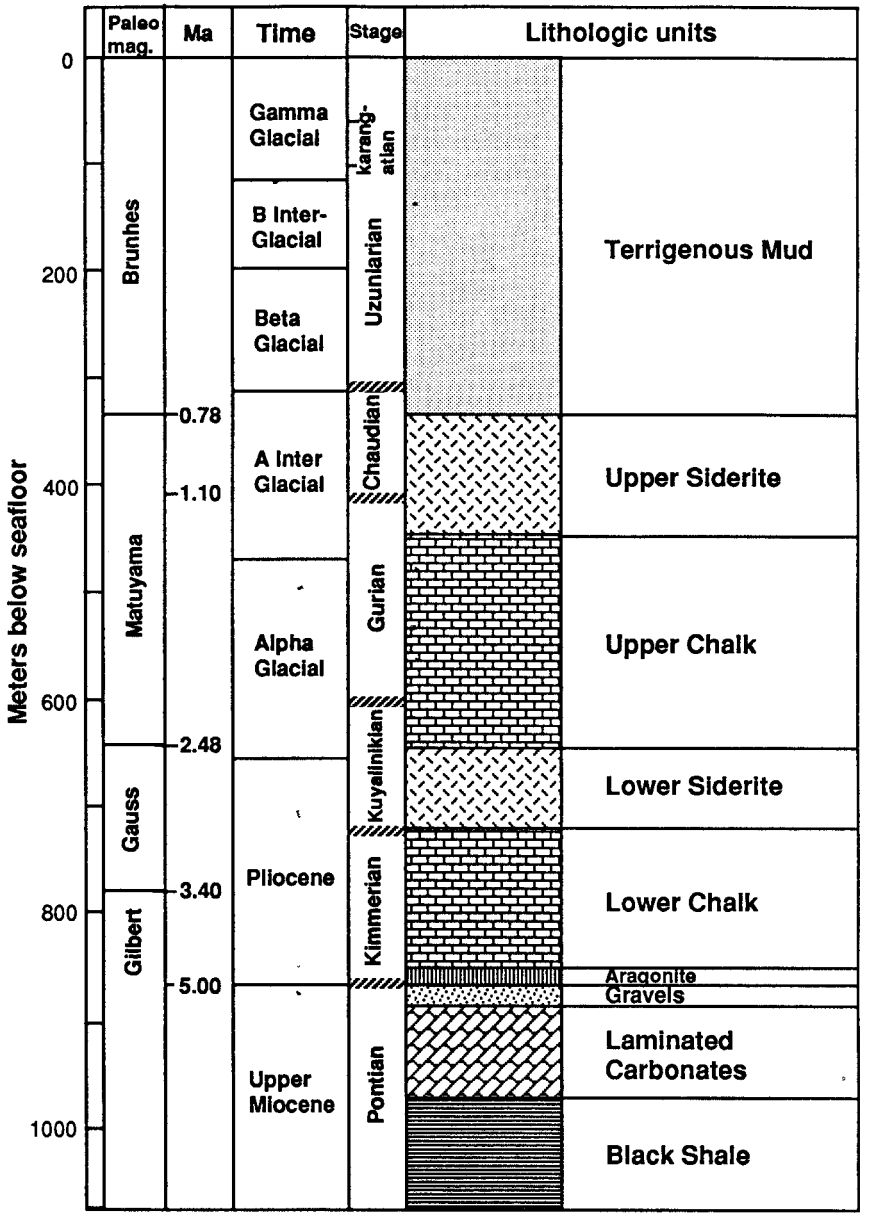

Fig. 2. Chronostratigraphy and history of changes in sedimentation in the Black Sea (DSDP Site 380). Magnetostratigraphic scale after Hsü and Giovanoli (1979), paleomagnetic ages after Harland and others (1990), Spell and McDougall (1992); lithostratigraphy after Hsü and Kelts (1978); and Black Sea continental stages after Zubakov and Borzenkova (1990). Zonation of the Quaternary record into three glacial intervals (Alpha, Beta, Gamma) and two interglacial periods after Traverse (1978) and Hsü (1978a). Correlation between Black Sea sedimentary record and continental sections has been done based on the paleomagnetic datums delineated in the deep sea cores by Hsü and Giovanoli (1979) and the magnetostratigraphic scale for the continental successions described by Zubakov and Borenkova (1990).

MODERN BLACK SEA

The Black Sea today is the world's largest land-locked inland sea (area: 423,000 km^2) and has a maximum depth of about 2200 m with an average depth of 1330 m. Thirty percent of the area of the basin is below a depth of 2000 m (Balkas and others, 1990). The sea is the catchment basin for a major portion of European fresh water discharge, and several important rivers drain into it. The basin is linked to the Mediterranean through the Bosporus Straits, a narrow conduit whose depth is about 36 m at present and has probably never exceeded 100 m (Zubakov and Borzenkova, 1990). Temporal and spatial variability of atmospheric conditions characterize the modern Black Sea climate. The highest average air temperatures are 24°C in the central and northern parts and 22°C in the southern parts of the basin. Mean annual surface water temperatures vary from about 16°C in the southern part, 13°C in the northeastern part, and 11°C in the northwestern portion of the basin (Balkas and others, 1990).

Although now located in a semi-arid climatic zone, the Black Sea is marked by a strong positive water balance. Precipitation and rivers provide about 550 km^3 of fresh water per year while only about 350 km^3 per yr are lost through evaporation (table 1). Most of the fresh water inflow is through drainage from continental areas, with the Danube River contributing nearly 60 percent of the total runoff. Brackish water from the Sea of Azov enters through the Kerach Strait as a surface current, and the more saline (S = 34), warmer Mediterranean water flows into the basin as underflow. In return, the relatively less saline (S = 18) surface waters of the Black Sea flow out via the Bosporus to the Mediterranean. Some Black Sea bottom water also flows northward into the Sea of Azov. Surface water salinities in the Black Sea range from 17.5 to 19, and below the halocline salinities average about 22. The halocline promotes vertical salinity stratification by hampering mixing between surface and bottom waters, with consequent water column anoxia below 80 to 200 m (variations in the depth of the oxic-anoxic interface reflect the balance between fresh water and salt water inflows; Murray and others, 1989).

TABLE 1

Hydrographic budget of the modern Black Sea (after Fonselius, 1974)

Gains		Losses	
Source	km^3 y^{-1}	Cause	km^3 y^{-1}
River input	320	Evaporation	350
Rainfall	230	Bosporus surface current	400
Bosporus subsurface current	200		
TOTAL	750		750

PLIO-PLEISTOCENE BLACK SEA

Physiography and Sedimentation History

The physical characteristics of the Black Sea developed into their present form during the late Quaternary. Considerable climatic fluctuations with corresponding sealevel changes during the last 6 to 8 my have left in their wake a record of extreme changes in the sedimentary regime. Over time, the Black Sea has also been subjected to changes in its hydrographic budget through variations in major drainage patterns, climatic perturbations of freshwater inputs, and rates of evaporation (Scholten, 1974; Degens and Paluska, 1979). In addition, several studies have shown that during the Tertiary and Quaternary, the Black Sea depositional environment vacillated between fresh water lacustrine and brackish-marine, because the sealevel in the Mediterranean repeatedly rose above or below the sill depth of the Bosporus (Degens and Ross, 1974, and papers therein; Hsü, 1978a, b; Hsü and Kelts, 1978; Schrader, 1978, 1979). Geological and geophysical data suggest that aside from a short interlude of basin desiccation in the late Miocene, the Black Sea remained a gigantic deep basin throughout the Cenozoic (Hsü and Giovanoli, 1979).

The history of sedimentation in the Black Sea includes black shale deposition during the late Miocene, followed by chemical carbonate sedimentation to the end of the early Quaternary, and a change to largely terrigenous sedimentation during the middle to late Quaternary (fig. 2). The modern phase of sedimentation in the basin is represented by finely laminated coccolith marl. Deposition of chemical sediments began in a fresh water basin, when the regional climate was warm and temperate, continued through a late Pliocene cooling trend and early Pleistocene glacial conditions, and terminated during an interglacial episode (Hsü, 1978a). As revealed at DSDP Site 380, the suite of chemical sediments consists of dolomite muds, magnesian calcite, aragonite, and millimeter to decimeter thick couplets of chalk/organic-carbon rich clays or marl, and sideritic mud/diatomaceous clay or marl (fig. 2). Correlation of lithology with paleoclimate suggests that the chalk units were deposited during relatively cold and dry condtions, and the sideritic mud units during warm and wet preglacial or interglacial periods (Hsü and Kelts, 1978).

Environmental and Hydrological Conditions during Siderite Deposition

In order to relate our thermodynamic model results to the Black Sea depositional system during the times of siderite deposition, it is necessary to gain some insight into the environmental and hydrological conditions characterizing the Black Sea during these periods. Because the siderite-rich sediments were primarily deposited during two relatively short time-spans in the Plio-Pleistocene, an understanding of the nature of the chemical environment and the factors that promoted siderite precipitation in the Black Sea basin is fundamental to the development of the

model. In particular, the following aspects of the Neogene Black Sea depositional system merit attention.

1. The climatic conditions characterizing the Black Sea region. To what extent were environmental conditions conducive to siderite deposition?
2. The nature of the Black Sea basin. Was it an isolated fresh water lake during times of siderite deposition or a lacustrine system with limited water exchange with the Mediterranean?
3. The hydrochemistry of waters draining into the Black Sea. Does the sedimentary record in the basin or the geology of the hinterland indicate that the rivers draining into the Black Sea during the times of siderite deposition were similar in composition to the Satilla waters we have used in developing our model?

In this section, we discuss the above aspects and show that environmental conditions and water chemistry during times of siderite deposition were indeed favorable for iron carbonate precipitation.

Climatostratigraphic constraints.—Paucity of chronostratigraphically diagnostic floral and faunal elements in the sediment cores has seriously hampered a proper stratigraphic evaluation of the Black Sea sediment sequences (see Schrader, 1978, 1979; Stoffers and Müller, 1978; and Hsü, 1978a and b, for three differing view points). Here, we accept Hsü's interpretations of Black Sea stratigraphy and sedimentation history based on pollen and diatom evidences, paleomagnetic data, climatic variations, and estimates of sedimentation rates (Hsü, 1978a; Hsü and Giovanoli, 1979). Correlation of the paleomagnetic stratigraphy for the sediments developed by Hsü and Giovanoli (1979) with their probable continental equivalents in the Black Sea region (Kerch-Taman, Azov, Danube, and Ukraine areas), as described by Zubakov and Borzenkova (1990), provides some important constraints on the climatic and hydrologic development of the Black Sea basin during deposition of the two siderite units. Some of the climatostratigraphic observations of relevance to the present study are summarized below.

Chronostratigraphy of the Black Sea sediment record shows that the lower siderite unit was deposited between about 3.0 and 2.5 Ma, corresponding to the Gauss Magnetic Epoch (fig. 2). In the marine section of the Eastern paratethys (which includes the Black Sea basin), this paleomagnetic epoch occurs in the Kuyalnikian regional stage (fig. 2). Paleoclimatic studies indicate that the early part of this stage was characterized by a warm, humid climate, as reflected in the meadow/brown forest paleosols and forest pollen record of the pedological sections found in the Ukraine (Zubakov and Borzenkova, 1990). In the Crimean valley, the dominant soils during this period were reddish brown in color, typical of subtropical forest areas (Sirenko and Turlo, 1986). Annual summer temperatures were of the order of 23° to 25°C, and precipitation rates were low (Sirenko and Turlo, 1986). On the eastern margin of the Black Sea, palynological data from Georgia indicate two warm and two cold phases during the Kuyalnikian. The warm periods centered around

approx 2.8 and 1.8 Ma were marked by a proliferation of polydominant conifers, hardwoods, ferns, and subtropical plants (Shatilova, Macharadze, and Davitashvili, 1991).

Hsü and Giovanoli (1979) identified a paleomagnetic datum horizon near the top of the upper siderite unit at 330 m below the present sea floor as corresponding to the Brunhes-Matuyama boundary at 0.78 Ma (fig. 2). In the Black Sea continental section, the Brunhes-Matuyama transition occurs within the Chauda regional stage (fig. 2). The Chauda stage ranges in age from 0.6 to 1.1 Ma (Zubakov and Borzenkova, 1990). If we accept the estimated rate of sedimentation of 18.5 cm/10^3 yrs for the upper siderite unit as given by Hsü and Giovanoli (1979), then most of the upper siderites correspond to the Chauda stage and to the underlying Gurian stage (fig. 2). The upper part of the Gurian stage, correlatable to the upper siderite unit, represents a warming phase in the Black Sea region, as reflected in the iron oxide-rich reddish brown buried paleosols of the period (Zubakov and Borzenkova, 1990). Pollen records also indicate the widespread existence of forests dominated by pines and other conifers. Mean winter air temperatures never dropped below 0°C, and precipitation was low (Zubakov and Borzenkova, 1990).

The Gurian-Chauda transition at about 1.1 Ma (fig. 2) was marked by the drainage of Caspian waters into the Black Sea and a consequent freshening of the basin. The Chauda climate in the Black Sea region was much warmer and wetter than at present, with a dominance of beech-coniferous forests and tropical ferns (Zubakov and Borzenkova, 1990). Mean winter and summer temperatures were also markedly higher than at present (Shatilova and Mchedlishvili, 1980). Lateritic soils characterize the pedological sections corresponding to the latter part of the Chauda.

Palynological studies of the Black Sea sediment cores by Traverse (1978) lend further support to the climatostratigraphic observations. The record of forest and steppe pollen preserved in the cores points to dramatically fluctuating climatic conditions in the Black Sea catchment area during most of the Neogene, with at least two major periods of relative warmth during the Plio-Pleisocene. The deposition of the two siderite units broadly corresponds to these times of warm climatic conditions in the hinterland and in the Black Sea basin (Hsü, 1978a, b).

Hydrographic constraints.—Zubakov and Borzenkova (1990) argue for a single rhythmic pattern reflecting climatic changes in the Caspian–Black Sea–Mediterranean system, although each of the three seas may have responded locally in its own way to any change. Unlike the Mediterranean-Black Sea system, the level of the Caspian Sea is controlled primarily by precipitation and not by glacial-interglacial episodes. Variations in Caspian Sea level are in general opposite in phase to the transgressions and regressions in the Mediterranean–Black Sea system (Zubakov and Borzenkova, 1990). Thus, during peak regressions in the Mediterranean, which would broadly correspond to periods of extensive transgressions in the Caspian, the Black Sea would be a through-flow lake and a part of the Caspian Sea. Isolation and development of

closed-basin hydrologic conditions in the Black Sea can therefore occur only during the early part of a transgressive phase (or end of a regressive phase) in the Mediterranean, because these periods will also be times of regression in the Caspian.

A climatostratigraphic correlation of the marine Pleistocene sequences of the Caspian, Mediterranean, and the Black Seas indicates that Chauda time largely corresponds to a regressive phase of Caspian waters with very little run-off into the Black Sea. Two major transgressions of the Caspian Sea into the Black Sea demarcate the upper and lower boundaries of the Chauda stage. As discussed previously, fresh water lacustrine conditions persisted in the Black Sea basin during the Chauda period, corresponding to the time of deposition of the upper siderite unit. Thus, it would appear that closed basin hydrological conditions characterized the Black Sea during most of the time of deposition of the upper siderite unit.

In contrast, a major part of the period of deposition of the lower siderite unit corresponds to a transgressive phase (the Akchagylian transgression) of the Caspian waters. Below the Gauss/Matuyama polarity reversal (2.48 Ma), a prominent regressive episode is discernible (Zubakov and Borzenkova, 1990). Diatom analyses of Black Sea cores indicate predominantly oligohaline (0-5 permil salinity) waters in the Black Sea basin during the deposition of the lower siderite unit (Schrader, 1978). Furthermore, the occurrence of abundant Chrysophyta opal cysts in several diatomaceous layers in the lower siderite unit indicates either the desiccation phase of a fresh water environment (Dahm, 1956, cited in Schrader, 1978) or at least restricted basinal conditions (Schrader, 1978). Thus, it is possible that there were occasional water exchanges between the Black Sea and the Mediterranean during the times of deposition of the lower siderite unit, when the Bosporus might have acted as an outflow conduit for Caspian waters draining into the Black Sea.

BLACK SEA SIDERITES

Because any thermodynamic model of a natural aqueous system tends to remain highly speculative unless the products of the model can be related to the mineralogy and geochemistry of the solid phases actually present in the system modeled, our laboratory studies of the siderite-rich horizons recovered from the Black Sea were primarily oriented toward obtaining information on the morphology of the siderite grains and the composition of the carbonate phases present. We also wanted to verify whether the silt-sized, wheat-shaped sideritic grains exhibit any textural features which might argue for an early diagenetic origin of these carbonates. In addition, we carried out carbon and oxygen isotopic analyses of the coexisting calcite and siderite in the siderite units to see whether the isotopic signatures also support our hypothesis of endogenic precipitation.

Siderites in the Plio-Pleistocene section of the Black Sea predominate in two mud-diatomaceous clay sequences, of thicknesses 114 and 73 m,

A.

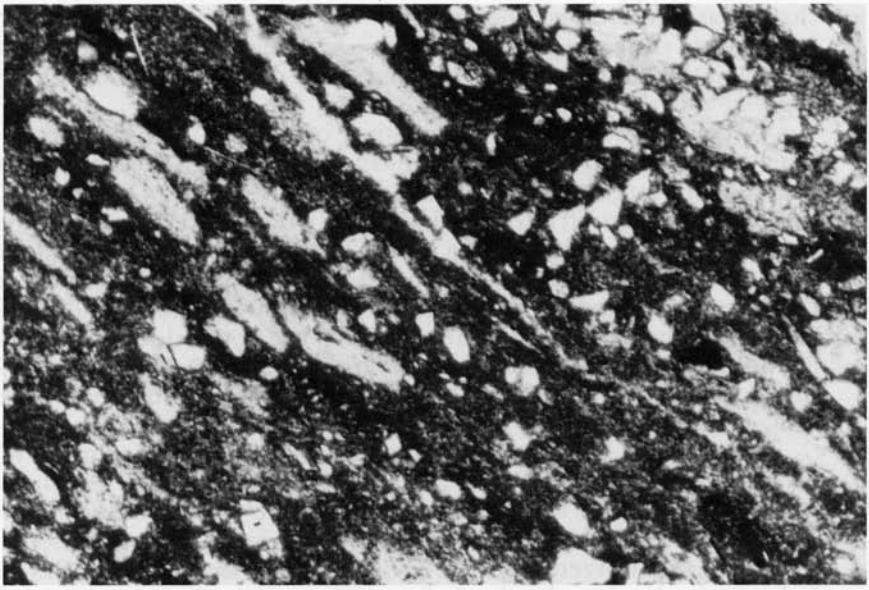

B.

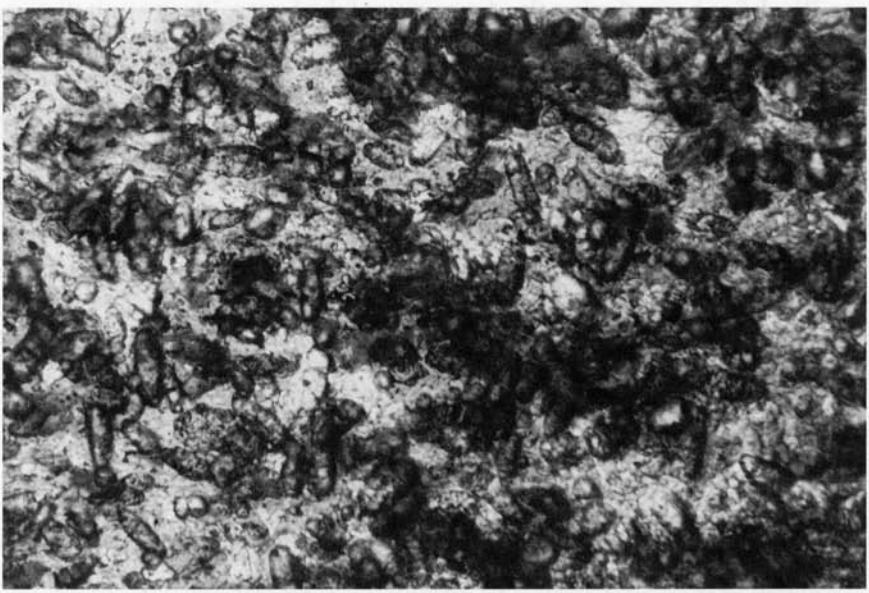

Fig. 3. Photomicrographs of siderite-bearing intervals. (A) Microlaminations in the upper siderite unit. The matrix is composed of subequal proportions of siderite, detrital quartz and clay. Plane polarized light. Horizontal dimension of the photo is 1.0 mm. Sample no. 380A-9-1/127-128 cm. (B) Euhedral, silt-sized, wheat-shaped grains of siderite in the upper siderite unit. Plane polarized light. Horizontal dimension of the photo is 0.21 mm. Sample no. 380A-8-5/146-147 cm.

C.

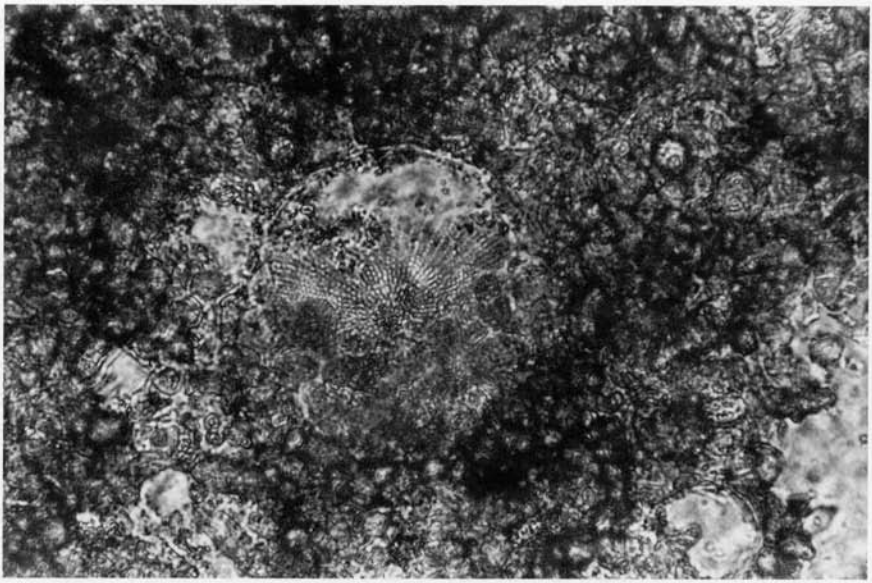

Fig. 3(C) Replacement of diatom tests by early diagenetic siderite. Small subhedral grains of siderite constitute the bulk of the groundmass. Plane polarized light. Horizontal dimension of the photo is 0.21 mm. Sample No. 380A-42-1/6-7 cm.

respectively, separated by a 198 m thick unit composed primarily of mud, marl, and chalk (fig. 2). In the upper unit, siderite commonly occurs as finely disseminated grains or as thin lithified laminae interbedded with terrigenous muds or marl (fig. 3A). The lower siderite unit, however, is marked by millimeter- to decimeter-thick (maximum thickness around 15 cm) interbeds of siderite, marls with siderite admixture, and diatomaceous clays. Thin horizons of alternating siderite and chalk are also characteristic of the upper chalk sequence that separates the two siderite units.

Mineralogy and Chemistry

Petrographic analyses of the sideritic mud show that in many cases siderite constitutes the bulk of the sediment. It occurs as reddish-brown, spindle-shaped, euhedral grains, either disseminated in the clays or confined to microbands in a siliciclastic matrix (fig. 3A, B). Grain sizes range from 1 to 10 μm. The presence of siderite concretions (mm to 5 cm in diam) with relict structures showing replacement of diatoms by siderite (fig. 3C) points to early diagenesis (Emelyanov and others, 1978). While we do not rule out early diagenetic precipitation of siderites in the Black Sea sediments (particularly for the larger concretionary masses), we are most interested in establishing whether the silt-sized grains of siderite dispersed throughout the mud/clay sequences could be endogenic pre-

cipitates or whether the fine disseminations, layers, beds, and concretions represent a transitional sequence of early diagenetic processes. We will return to this topic later.

For a qualitative assessment of the gross mineralogy of the sideritic mud and interbeds, X-ray diffraction analyses were performed on smear slide samples of these lithologies from core 380A. The diffraction patterns of the sideritic muds show peaks characteristic of siderite and calcite associated with an illite–chlorite–quartz–feldspar assemblage. Calcite-rich intervals with less than 5 percent siderite are also characteristic of some interbeds. Reddish-brown, decimeter-thick interbeds and concretionary siderites, however, tend to be relatively pure siderite.

Quantitative electron microprobe analyses of the mineral assemblages in the sideritic muds were also carried out with particular emphasis on the carbonate constituents. Al and Si were included as a check for detrital interference. Results are given in figure 4. These data indicate that the siderite grains have a mixed carbonate composition with varying amounts of Fe, Mg, Ca, and Mn. Total iron content averages 31 percent, compared with 48.2 percent for stoichiometric $FeCO_3$. Spot analyses on the spindle-shaped grains do not show any noticeable variation in composition within a single grain. The results also show a distinct compositional difference between the two siderite units. Relative to the upper siderite unit, the siderites of the lower unit are enriched in iron and manganese and depleted in calcium and magnesium (fig. 4).

Stable Isotopic Composition

Samples of sideritic mud from the two siderite units and from the siderite-rich chalk-marl cycles in the upper chalk unit were analyzed to determine their $\delta^{13}C$ and $\delta^{18}O$ compositions. Carbon dioxide was extracted selectively from siderite by reacting pretreated samples in anhydrous phosphoric acid (density > 1.9 gm cm^{-3}) at 50°C for over 48 hrs. Although such short reaction times may not provide quantitative yields of CO_2 from siderites, incomplete reactions have been demonstrated to introduce only insignificant errors in the isotopic compositions of siderites (Aharon, 1988; Beukes and others, 1990; Moore, Ferrell, and Aharon, 1992). Prior to reaction with phosphoric acid, siderites were treated with 5 percent acetic acid to remove associated calcium carbonate, if present (compare Cortecci and Frizzo, 1993). Oxidizable organic matter was removed by treating the samples with a 4 percent NaOCl solution for 16 hrs. The difference in reactivity between siderite and calcite to H_3PO_4 was used in extracting the CO_2 from a limited number of samples containing both phases. Bulk samples were first treated with phosphoric acid at 25°C for 2 hrs, and the resulting CO_2, corresponding to calcite, analyzed for its isotopic composition. X-ray diffraction of samples reacted in a similar manner indicates that such a treatment apparently has no effect on the coexisting siderite grains. The reaction vessel was then transferred to a water bath at a temperature of 50°C, and the CO_2 collected from siderite. Oxygen isotopic compositions of siderite determined by this process as

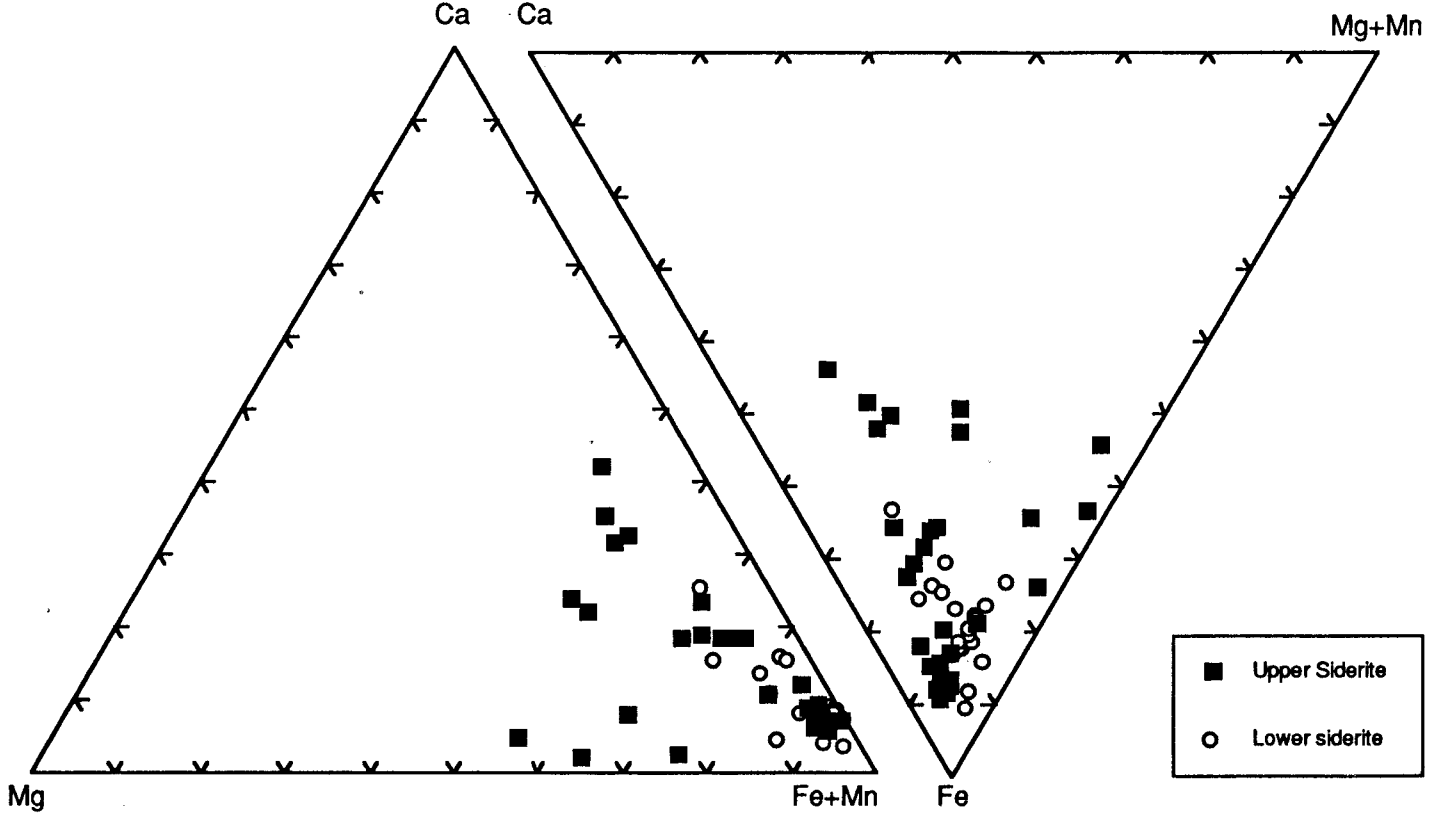

Fig. 4. Range of elemental composition of siderites (expressed as molar percentages of the oxides) in the two siderite units. Filled squares, siderites in the upper siderite unit. Open circles, siderites in the lower siderite unit.

well as the results from acetic acid-treated samples from the same horizon agree within ±0.5 permil. Oxygen isotopic values of siderites were calculated using a fractionation factor of 1.01075 (Carothers, Adami, and Rosenbauer, 1988), and the results given in the conventional delta notation with respect to PDB.

The carbon and oxygen isotopic compositions of the carbonate phases in the two siderite units as well as from the siderite-chalk interval in the upper chalk unit are shown in figure 5. Two distinct populations are characteristic of the $\delta^{13}C$ values of siderites. The extremely positive $\delta^{13}C$ values of 9 to 15 permil for the concretionary siderites are suggestive of a CO_2 source strongly enriched in ^{13}C. Organic matter degradation in the zone of methanogenesis appears to be the most likely process responsible for this ^{13}C enrichment; carbon isotopic fractionation in the methanogenesis zone can result in $\delta^{13}C$ values up to 15 permil in the CO_2

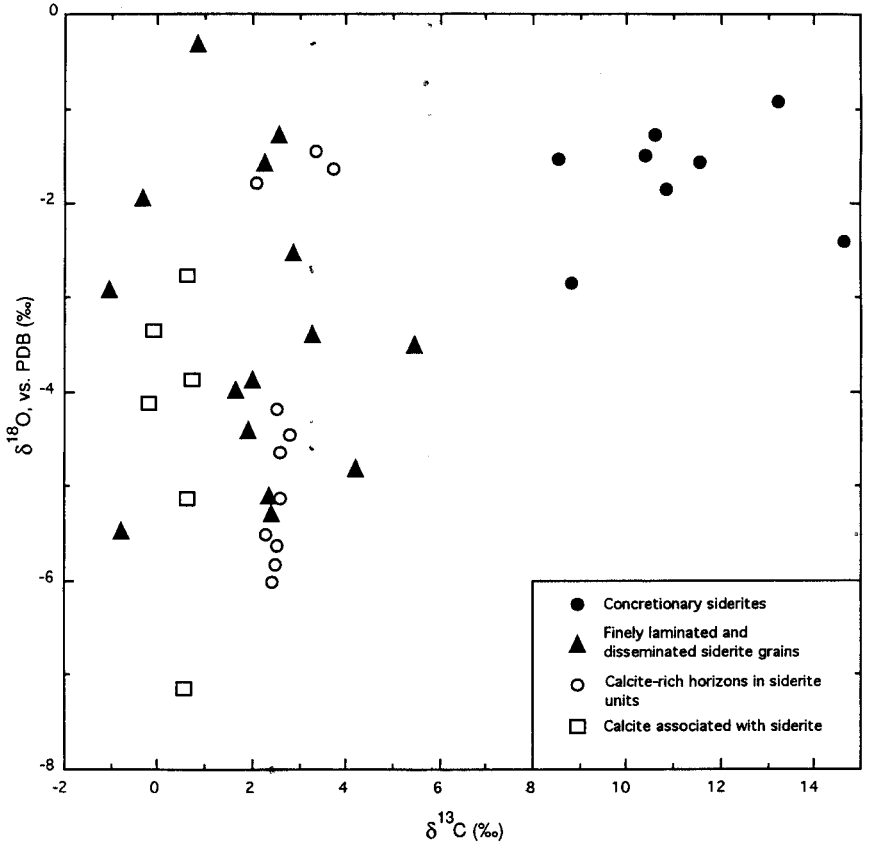

Fig. 5. Cross plot of $\delta^{13}C$ and $\delta^{18}O$ of siderite and calcite in Black Sea siderite units.

byproduct (Irwin, Curtis, and Coleman, 1977; Whiticar, Faber, and Schoell, 1986). Indeed, petrographic studies of these siderite samples show evidences of replacement of diatoms by siderite, pointing to early diagenesis. In marked contrast, the carbon isotopic values of disseminated and laminated siderite grains range from −0.35 to +4 permil. In terms of early diagenesis, the observed variations in the isotopic composition of the finely disseminated and laminated siderite grains could result from either of the following processes:

1. Siderite precipitation under suboxic conditions in the zone of Fe^{3+} reduction (Maynard, 1982; Walker, 1984).
2. Mixing, in the pore waters or at the sediment-water interface, of ^{13}C-enriched CO_2 from methane fermentation and ^{13}C-depleted CO_2 produced by microbial destruction of organic matter.

There is also a third possibility. Siderite precipitating in equilibrium with the dissolved inorganic carbon (DIC) pool in an anoxic water column with low dissolved sulfide concentrations can be expected to have a carbon isotopic composition near 0 permil, typical of primary carbonates (Golyshev, Padalko, and Pechenkin, 1981; Maynard, 1982). Below, we examine whether the relatively light carbon isotopic signature of the disseminated and laminated siderite grains could be the result of their precipitation from the water column.

Geochemical studies of the two chalk units in the Plio-Pleistocene Black Sea (fig. 2) indicate that the calcites in these units are predominantly inorganic surface water precipitates formed during episodes of enhanced primary productivity (Hsü, 1978; Hsü and Kelts, 1978; Glenn and others, 1992). The presence of both laminated and bioturbated cycles of marl-chalk in this unit also point to periodically (seasonally?) stagnant, oxygen-deficient bottom waters alternating with times of oxygenation. The calcite-rich interbeds in the siderite units have carbon isotopic values comparable to those of the calcites in the two chalk units (mean $\delta^{13}C = 2.6$ permil; Deuser, Degens, and Stoffers, 1978; work in progress), suggestive of their precipitation by a similar process.

If the carbon isotopic signature of the calcites in the Black Sea reflects the dissolved carbon isotopic composition of the basin waters, the question to be raised here concerns the significance of the isotopic values of the disseminated and finely laminated siderites, which plot in the range of −0.35 to +4 permil (fig. 5). A close inspection of the $\delta^{13}C$ values indicates two broad fields, defined by values close to 0 permil and between 2 to 0 permil. The calcites *coexisting* with the siderites have $\delta^{13}C$ values close to 0 permil. The lighter isotopic composition of the siderites and the coexisting calcites could be explained as having resulted from mixing of organically derived ^{13}C-depleted CO_2 with the DIC having a $\delta^{13}C$ composition of about 0 permil. Relative to the coexisting calcites, however, siderites with a mean $\delta^{13}C$ value of 2.7 permil show enrichment in ^{13}C by 0.5 to 2.0 permil, that is, $\Delta\delta^{13}C_{\text{siderite-calcite}} = 0.5$ to 2.0 permil (fig. 5). Theoretical calculations of Golyshev, Padalko, and Pechenkin (1981) predict an enrichment in the carbon isotopic composition of siderites by

about 5 permil, if both calcite and siderite precipitate from the same water mass at 25°C. The reason for the primary difference between the theoretical value and the observed variations in $\Delta\delta^{13}C_{siderite\text{-}calcite}$ is, however, not well constrained by the data.

MODEL METHODOLOGY

Our discussions so far highlight the fact that environmental conditions of the Black Sea area and the water chemistry of the basin were highly favorable for precipitation of siderite during specific time intervals. In this section, we examine whether, given a feed water of a certain composition, isothermal evaporation of this water at 25°C in equilibrium with atmospheric CO_2 can precipitate siderite of the observed composition and textural characteristics. Fundamental to our model is the choice of river water composition, as constrained by the climatic and terrestrial ecosystem conditions prevalent in the Black Sea area during the times of siderite precipitation. Thus, the development of the thermodynamic model involves four stages: (1) establishing that the feedwaters of the Black Sea during times of siderite deposition were similar in composition to the present-day Satilla river system of the southeastern United States; (2) calculation of the changes in composition of these waters as they are progressively evaporated isothermally at 25°C; (3) determination of the compositions of the various carbonate phases that precipitate at different concentration levels; and (4) evaluation of the model results in terms of the observed textural characteristics of the siderite-rich horizons in the Black Sea sediments.

Choice of Feedwater

Table 2 gives the average analytical concentration of the Satilla drainage system of the southeastern United States. The Satilla river system is remarkably similar in hydrology and basinal characteristics to the postulated hydrologic and environmental conditions in the Black Sea catchment area during the times of deposition of the siderite units. The Satilla river lies entirely within the coastal plain, and its basin is characterized by poorly-drained acidic soils and reddish-yellow latosols (Beck, Reuter, and Perdue, 1974). Latosols are the products of deep chemical weathering and are the most heavily weathered and leached soils in the world (Warman, 1964). Similar iron-rich, reddish yellow lateritic soils also mark the Chauda Stage of the Black Sea continental stratigraphic sections. Swamps abound in the Satilla drainage basin, and much of the drainage is over low-relief topography (Beck, Reuter, and Perdue, 1974). Humid wet-dry subtropical climate, similar to the Black Sea climate during the times of siderite deposition (discussed above), is typical of the catchment areas of this river system. Temperatures are high, with an annual mean of 16° to 20°C; however, sharp gradients exist between the summer and the winter (Warman, 1964). Hardwood deciduous forests with slash pines, typical of warm, humid environments, are prevalent in the drainage area (Walker, 1991).

TABLE 2

Mean chemical composition of the Satilla drainage system (Beck, Reuter, and Perdue, 1974) and the composition of the water used in the evaporation model*

Concentrations in ppm			
HCO_3	2.61	Ca	1.32
Cl	6.11	SiO_2	6.61
SO_4	0.84	Al	0.41
Na	3.70	Fe	1.05
K	0.96	Mn	0.06
Mg	0.74	NO_3	1.00

Composition of the water used in this study		
	ppm	$\times 10^{-5}$ moles/liter
H_4SiO_4	6.61	6.88
Ca^{2+}	1.32	3.29
Mg^{2+}	0.74	3.04
Na^{+}	3.70	16.10
K^{+}	0.96	2.46
Fe^{2+}	1.05	1.88
Mn^{2+}	0.06	0.19
HCO_3^{-}	4.10	6.72
SO_4^{2-}	0.84	0.87
Cl^{-}	9.69	27.30

* Mean composition of 18 river water samples analysed; average pH = 4.59.

The Satilla waters are characterized by a relatively low suspended load (only a few tens of ppm), an abundance of dissolved organic carbon, and low pH (3.8-5.9, avg 4.6). The main constituents of the river water organic matter are humic substances, resembling soil fulvic acids (Beck, Reuter, and Perdue, 1974). Besides controlling the pH of the waters, these humic substances can be expected to influence the aquatic concentration of soluble metal ions because of complexation, or colloidal association, or a combination of both processes (see discussion below). Most of the iron and aluminum in the Satilla waters is present as either dissolved or colloidal metal-organic complexes (Beck, Reuter, and Perdue, 1974; Perdue, Beck, and Reuter, 1976).

Evaporative Concentration of the Basin Water

Composition of the basin water.—The composition of the waters assumed to be entering the Black Sea basin during the times of siderite deposition is given in table 2. This composition has been modified from the average analytical concentration of the Satilla drainage and conforms to several constraints. Beck, Reuter, and Perdue (1974) showed that the electrical imbalance between the analytical anion and cation concentrations in their data could be corrected by considering dissociated carboxylate anions in the charge balance. However, because the structural characterization and concentration of the various functional groups in the river water humic substances are not adequately known, incorporation of the

organic ligands into thermodynamic models may not be realistic (Reuter and Perdue, 1977). Therefore, in the analytical concentration we have assumed for the composition of the feedwater, the electrical imbalance has been corrected by increasing the analytical concentration of (Cl^- + NO_3^-) from 7.11 ppm to 9.69 ppm. This correction does not affect our evaporation path calculations. Furthermore, as we discuss later, the concentrations of organic anions *per se* do not significantly alter our model results. Similarly, we have used a HCO_3^- concentration of the feedwaters into the Plio-Pleistocene Black Sea as equal to 4.1 ppm (the reported average value of Satilla water is 2.6 ppm), chiefly to facilitate the calculations at high evaporative concentrations. The value we have adopted in fact corresponds to the average bicarbonate concentration of Satilla water in its upper reaches. The implications of varying the HCO_3^- concentration are also discussed in a later section. We also ignore aluminum in our calculations, consider H^+ as a species, and the reported silica (SiO_2) concentrations as H_4SiO_4.

The basis for treating the reported concentration of iron in the Satilla waters as free, dissolved Fe^{2+} needs some discussion. In natural waters, iron is found in both Fe (II) and Fe (III) states (Davison, 1993). Ferrous iron, Fe^{2+}, is the more soluble of the two species, but because it is readily oxidized and precipitated as Fe (III) oxyhydroxide, especially at higher pH, the stability of ferrous iron is limited in typical, well oxygenated, freshwaters (Miles and Brezonik, 1981; Davison, 1993). However, certain naturally occurring organic materials of humic origin have been shown to retard the rate of oxidation of Fe^{2+} in many aerobic freshwater systems through reducing and complexation reactions (Shapiro, 1964; Ghosh, O'Connor, and Engelbrecht, 1967; Theis and Singer, 1973, 1974; Koenings, 1976; Miles and Brezonik, 1981). Laboratory experiments suggest that this inhibition of the rate of ferrous iron oxidation results from a complexation–oxidation–reduction cycle mediated by organic ligands and light (Morgan and Stumm, 1964; Theis and Singer, 1974; Miles and Brezonik, 1981; Waite and Morel, 1984; Sulzerberger and others, 1989). Briefly, the sequence of reactions involves the following steps (fig. 6):

1. Complexation reactions leading to the formation of ferrous-organic ligand complexes. The fraction of ferrous iron complexed depends on the pH of the water and the nature and concentration of the organic ligand.

2. Slow oxidation of the Fe(II)-humic complex and any free Fe(II) to Fe(III)-humic complex and Fe(III), respectively. The free Fe(III) formed is also strongly complexed by humic material present in the system (Miles and Brezonik, 1981). The rate of oxidation of the complexed ferrous iron is highly dependent on the pH (being higher in neutral pH waters than in acidic ones) and the type and concentration of the organic ligand. Thus, for instance, tannic acid has been shown to retard completely the oxidation of Fe (II), while citric acid accelerates its oxidation (Stumm and Lee, 1961; Theis and Singer, 1974). Humic acid also inhibits ferrous iron

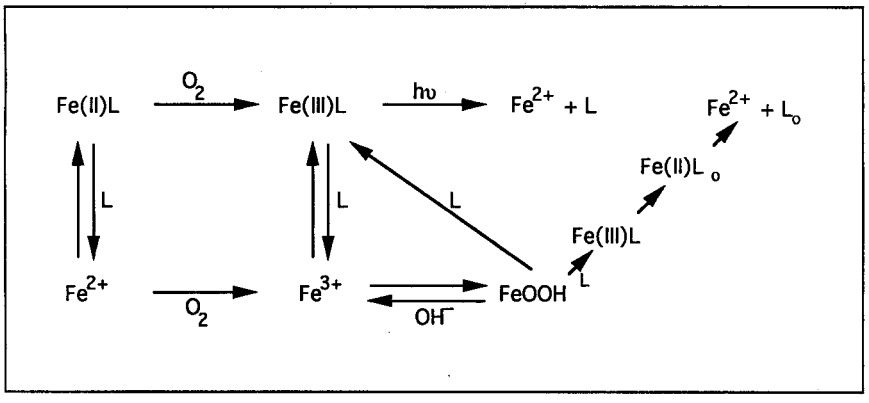

Fig. 6. The processes involved in the reduction of iron in oxygenated aquatic systems in the presence of organic matter. L and L_0 represent, respectively, the ligand and its oxidized form (after Theis and Singer, 1974; Davison, 1993).

oxidation, especially at higher acid concentrations and at lower pH values (Miles and Brezonik, 1981).

3. Reduction of the resultant unstable Fe(III)-humic complex to Fe(II) complex by humic matter, at even neutral pH in the dark, the reduction occurring more rapidly in the light. The rate of reduction also is a function of the type of organic ligand complexed with the iron. The Fe(II)-organic complex formed is unstable, dissociates, and liberates free Fe^{2+} and oxidized organic matter, thus continuing the cycle (Theis and Singer, 1974; Miles and Brezonik, 1981). If conditions are such that the rates of Fe(III) reduction and dissociation are rapid in comparison to oxidation rates, a relatively high steady-state concentration of ferrous iron can be maintained even in oxygenated aquatic systems, as long as the proper organic compounds are available to reduce Fe(III).

Another sequence of ligand-catalyzed photochemical oxidation-reduction reactions involving ferric iron and hydroxyl groups simultaneously operates in freshwater aquatic systems (compare Sulzerberger and others, 1989; Hering and Stumm, 1990). Because Fe(III) is easily hydrolyzed, the ferric iron resulting from the oxidation of Fe^{2+} or Fe(II)-humic complexes can either be complexed by organic ligands or form colloidal Fe(III) oxyhydroxide, depending on the pH and the nature and concentration of the organic ligand. At low pH and in the presence of suitable organic ligands, the Fe(III) oxyhydroxide phase readily undergoes reductive dissolution through photochemical processes (McKnight, Kimball, and Bencala, 1988; Sulzerberger and others, 1989). Such dissolution reactions can also occur at higher pH values but at lower rates and in the presence of such reductants as diphenols, hydroxycarboxylates, et cetera (Sulzerberger and others, 1989). Biologically-mediated processes have also been demonstrated to be capable of

influencing the dissolution-precipitation cycle of iron (Arnold, Di Christina, and Hoffmann, 1988).

In light of the above discussions, it seems reasonable to expect that a significant portion of iron in the low-pH, humic-compound-rich Satilla waters is present as either free Fe^{2+} or as dissolved or fine colloidal ferrous-organic (humate) complexes and Fe(III) oxyhydroxides. In the oxygenated surface waters of a depositional basin, the ferrous and ferric complexes may participate in organic ligand-catalyzed photochemical redox reactions, maintaining a relatively high steady-state concentration of Fe(II). Although the rates of reaction are likely to be very slow at the relatively high pH values of siderite precipitation (see below), this may not be limiting the availability of free Fe^{2+} for siderite precipitation. Thus, in considering the analytical concentration of the feedwaters entering the Black Sea depositional basin, we have assumed that the total analytical concentration of iron in the Satilla represents free Fe^{2+}. This concentration is probably a maximum bound, but, as we discuss later, even if only a third of the total iron concentration is present as free, dissolved Fe^{2+}, the reaction pathways for components of our evaporation model are not significantly affected.

It is worthwhile at this stage considering what happens to the organic component of the riverine waters entering the Plio-Pleistocene Black Sea evaporatory basin during the formation of the siderite units. Most present-day freshwater and coastal marine ecosystems (prior to human impacts) are net exporters of CO_2 to the atmosphere (Garrels and Mackenzie, 1971, 1972; Smith and Mackenzie, 1987; Wollast and Mackenzie, 1989; Smith and Hollibaugh, 1993; Cole and others, 1994). The CO_2 flux across the coastal sea-air interface results from the precipitation of calcium carbonate and/or net ecosystem production (NEP) in which the rate of respiration and decay of organic matter exceeds that of organic production. In most freshwater aquatic systems, the CO_2 degassing flux is maintained both by CO_2 derived from plant root and soil respiration and imported to the system by surface or ground waters and by increased respiration within the water body of allochthonous organic materials derived from the catchment basin. Although there are some uncertainties in the analytical data, the mean partial pressure of CO_2 in rivers and lakes averages about ten and three times respectively, that of the atmosphere (Garrels and Mackenzie, 1971; Cole and others, 1994).

An ecosystem with a negative NEP is heterotrophic and consumes more organic matter than it produces. Many aquatic systems, including most freshwater and coastal marine environments, are heterotrophic. Heterotrophic conditions characterize aquatic environments with strong inputs of reactive organic matter in the form of particulate and dissolved organic carbon (POC and DOC) (Smith and Hollibaugh, 1993; Cole and others, 1994; Ver, Mackenzie, and Lerman, 1994). Thus, although it is difficult to document quantitatively, we feel it is a reasonable possibility that the Plio-Pleistocene Black Sea evaporatory basin was a net heterotrophic system, with the heterotrophy sustained by the oxidation of the

reactive DOC and POC transported to the basin by the Satilla-like river waters of the time. Certainly, the present-day Satilla river system is net heterotrophic as attested to by its high average internal CO_2 pressure of about $10^{-1.6}$ atm. In the Plio-Pleistocene Black Sea evaporatory basin, the organic- and iron-rich, low pH input waters would degas CO_2 as they came to equilibrium with atmospheric CO_2, and some portion of the organic matter, including organic ligands, ultimately would be oxidized to dissolved organic carbon. Under such conditions because of the kinetics of Fe^{2+} discussed above, moderately high Fe^{2+} concentrations could be attained and maintained in the basin waters undergoing evaporation and lead to siderite precipitation.

Calculation methodology.—Several assumptions are made in development of our evaporative concentration model. During evaporation, the basin waters are assumed to be isolated from reactions with the country rocks or solid alteration products. The water is assumed to evaporate isothermally at 25°C in equilibrium with atmospheric CO_2 ($10^{-3.5}$ atm). Any solids that formed are considered to remain in equilibrium with the water. The general procedure we adopted was to calculate the effects of concentrating the waters under the above conditions by various factors up to 1000, determine the stages at which different carbonate phases could precipitate out of the system, and keep track of the progressive effects of this precipitation on the pH and composition of the remaining waters (Garrels and Mackenzie, 1967; Hardie and Eugster, 1970, for further discussion of this approach). The solid phases we considered as likely precipitates from evaporation are siderite, rhodochrosite, calcite, hydromagnesite, and amorphous silica. Equilibrium constants for these phases are given in table 3. As we show later, even at 1000× concentration of these waters, the low sulfate and chloride concentrations preclude the formation of gypsum, anhydrite, halite, and other common minerals of evaporite deposits. Furthermore, because we are dealing with an oxygenated aquatic system and its response to varying intensities of evaporation, sulfate reduction and the consequent formation of pyrite and other iron sulfides can be ruled out. In our calculations, dissolved

TABLE 3

Equilibrium constants of solids considered as possible precipitates in the evaporation model and of carbonate minerals used in construction of the phase diagram

Species		pK	Source
Calcite	$CaCO_3$	8.46	Plummer and Busenberg, 1982
Siderite	$FeCO_3$	10.80	Bruno, Wersin and Stumm, 1992
Rhodochrosite	$MnCO_3$	10.58	Jakobsen and Postma, 1989
Hydromagnesite	$Mg_4(CO_3)_3(OH)_2$	36.47	Morse and Mackenzie, 1990
Amorphous silica	$SiO_2 \cdot 2H_2O$	2.70	Garrels and Mackenzie, 1967
Ankerite	$(Ca, Fe)(CO_3)_2$	9.96	Woods and Garrels, 1992
Kutnahorite	$(Ca, Mn)(CO_3)_2$	9.92	Mucci, 1988

silica is permitted to increase in concentration until saturation with respect to amorphous silica was attained. Obviously, such arbitrary buffering does not affect our modeling of the carbonate system; furthermore, in the case of the Plio-Pleistocene Black Sea, siliceous organisms, chiefly diatoms, were responsible for silica uptake from the waters. Thus, it is likely that dissolved silica concentrations did not reach saturation with respect to amorphous silica.

The initial step in the procedure is determination of the P_{CO_2} of the recomputed water analysis from the equation

$$P_{CO_2} = \left(\frac{a_{HCO_3^-} a_{H^+}}{K_H K_1}\right) = \left(\frac{m_{HCO_3^-} \gamma_{HCO_3^-} a_{H^+}}{K_H K_1}\right) \quad (1)$$

a_{H_2O} is taken as unity. K_H (Henry's Law Constant) = $10^{-1.468}$; K_1 = $10^{-6.352}$; $K_2 = 10^{-10.329}$ (Morse and Mackenzie, 1990).

Because of the very low ionic strength of the water, activity coefficients (γ_i) are calculated using the Davies equation

$$\log \gamma_i = -0.5 z_i^2 f(I) \quad (2)$$

where

$$f(I) = \left[\frac{I^{1/2}}{1 + I^{1/2}} - 0.2I\right]\left[\frac{298}{(t + 273)}\right] \quad (3)$$

and I is the ionic strength, z is the charge, and 't' is the temperature in °C (good over the range of about 0° to 50°C; Morse and Mackenzie, 1990). The ionic strength of the recalculated Satilla water is 0.00045, and P_{CO_2} is $10^{-1.61}$ (that is, the water is not in equilibrium with an atmospheric P_{CO_2} of $10^{-3.5}$ atm). At an evaporative concentration of 1000×, the ionic strength is only 0.27; thus, the use of the Davies equation is suitable over the range of evaporative ionic strengths of interest.

In order to determine the pH and accompanying changes in dissolved carbonate species as this water comes to equilibrium with atmospheric P_{CO_2}, we recast the electrical neutrality equation in such a way that pH-dependent species are to the right

$$2m_{Ca^{2+}} + 2m_{Mg^{2+}} + 2m_{Fe^{2+}} + 2m_{Mn^{2+}} + m_{Na^+} + m_{K^+} - 2m_{SO_4^{2-}} - m_{Cl^-} = m_{HCO_3^-} + 2m_{CO_3^{2-}} + m_{OH^-} - m_{H^+} \quad (4)$$

where

$$m_{HCO_3^-} = \frac{P_{CO_2} K_H K_1}{\gamma_{HCO_3^-} a_{H^+}} \quad (5)$$

$$m_{CO_3^{2-}} = \frac{P_{CO_2} K_H K_1 K_2}{\gamma_{CO_3^{2-}} a_{H^+}^2} \quad (6)$$

$$m_{OH^-} = \frac{K_{H_2O}}{\gamma_{OH^-} a_{H^+}} \tag{7}$$

$$m_{H^+} = \frac{a_{H^+}}{\gamma_{H^+}} \tag{8}$$

Through substitution of eqs (5), (6), (7), and (8) and the values for K in eq (4), the charge balance expression becomes

$$\frac{10^{-11.32}}{\gamma_{HCO_3^-} a_{H^+}} + \frac{2(10^{-21.649)})}{(\gamma_{CO_3^{2-}} a_{H^+}^2)} + \frac{10^{-14}}{\gamma_{OH^-} a_{H^+}} - \frac{a_{H^+}}{\gamma_{H^+}} =$$

$$2m_{Ca^{2+}} + 2m_{Mg^{2+}} + 2m_{Fe^{2+}} + 2m_{Mn^{2+}} + m_{Na^+} + m_{K^+} - 2m_{SO_4^{2-}} - m_{Cl^-} \tag{9}$$

The right-hand side of the expression is known from the water analysis data, and γ for the different species is computed from the Davies equation. Thus, expression (9) can be used to calculate the new pH of the water in equilibrium with atmospheric P_{CO_2} at 25°C, which is 7.10. From this value of the pH, the values for $m_{HCO_3^-}$, $m_{CO_3^{2-}}$, m_{H^+}, and m_{OH^-} are obtained, and the total water analysis determined. Although for a given initial concentration, computation of the activity coefficients is straightforward, for each subsequent concentration, we need to know the ionic strength I to calculate γ. However, this I, in turn, is dependent on the molality of the dissolved species which is what we are trying to compute. The method of solution of the problem is the standard one of sequential iteration: (1) for a given degree of evaporative concentration, the ionic strength is first estimated, that is, if the water concentration is twice the initial concentration, the ionic strength is estimated to be twice the initial I, et cetera; (2) then the tentative activity coefficients of the various species are determined using this I; (3) the approximate pH is obtained; (4) using this pH, we recalculate m_i for the pH-dependent species using eqs (4), (5), (6), (7), and (8); (5) the charge balance eq (9) is reiterated using the new values of m; and (6) the process is repeated until the pH difference between successive iterations is ≤ 0.01.

The next step in our calculation is to calculate, at the particular evaporative concentration, the proportions of each major component that exists as the free ion, as well as the proportion present as inorganic complexes. To determine the complexation of the major constituents, we followed the classic iterative solution scheme developed by Garrels and Thompson (1962) in their model of the speciation of seawater. The components we chose for the calculations are the metals Na^+, K^+, Ca^{2+}, Mg^{2+}, Fe^{2+}, and Mn^{2+}, and the ligands OH^-, HCO_3^-, CO_3^{2-}, SO_4^{2-}, and Cl^-. The equilibrium formation constants of the various aquatic complexes considered are given in table 4.

Briefly, the iteration scheme for calculating the distribution of major dissolved inorganic species in the feedwater involves the following steps: (1) the initial calculation is done by assuming that the principal compo-

TABLE 4

Equilibrium formation constants of aquatic species used in this study (data from Nordstrom and others, 1990)

Equilibria	log K
$Ca^{2+} + SO_4^{2-} = CaSO_4^0$	2.30
$Ca^{2+} + HCO_3^- = CaHCO_3^+$	1.11
$Ca^{2+} + CO_3^{2-} = CaCO_3^0$	3.22
$Mg^{2+} + SO_4^{2-} = MgSO_4^0$	2.37
$Mg^{2+} + HCO_3^- = MgHCO_3^+$	1.07
$Mg^{2+} + CO_3^{2-} = MgCO_3^0$	2.98
$Fe^{2+} + SO_4^{2-} = FeSO_4^0$	2.25
$Fe^{2+} + HCO_3^- = FeHCO_3^+$	2.00
$Fe^{2+} + CO_3^{2-} = FeCO_3^0$	5.50
$Mn^{2+} + SO_4^{2-} = MnSO_4^0$	2.25
$Mn^{2+} + HCO_3^- = MnHCO_3^+$	1.95
$Mn^{2+} + CO_3^{2-} = MnCO_3^0$	4.90
$Na^+ + SO_4^{2-} = NaSO_4^-$	0.70
$Na^+ + HCO_3^- = NaHCO_3^0$	0.25
$Na^+ + CO_3^{2-} = NaCO_3^-$	1.27
$K^+ + SO_4^{2-} = KSO_4^-$	−0.85
$Fe^{2+} + Cl^- = FeCl^+$	0.14

nent concentrations are equal to their respective total concentrations, (2) the concentration of each species, both free and complexed, is then calculated from the mass balance relation for each analyzed constituent, (3) the sum of the species in each mass balance equation is then compared to the total concentration, and the original assumption corrected in terms of the results obtained for the next iteration, and (4) the iteration continued till there is convergence (Garrels and Thompson, 1962; Garrels and Christ, 1965, for a detailed discussion of this approach). For our assumed feedwater composition, the calculation converges in three iterations.

At the initial concentration and ionic strength of the feedwater, the calculations show that inorganic complexes are of little importance. However, as the water comes to equilibrium with atmospheric CO_2 and is evaporated to higher concentrations, the effect of association among major ions becomes quite important. Thus, for instance, at an evaporative concentration of 12×, corresponding to siderite saturation, a substantial fraction of carbonate (94.5 percent) is complexed by iron (table 5). At still higher evaporative concentrations, calcium and magnesium sulfate complexes become significant.

After calculating the distribution of the major dissolved inorganic species in the water at a particular evaporative concentration, the total

TABLE 5

Distribution of major inorganic, dissolved species in the feedwater at an evaporative concentration of 12X. I = 0.005, pH = 8.2, and $P_{CO_2} = 10^{-3.5}$ atm. (M = cation, X = anion)

Ion	Molality (Total) moles kg^{-1}	% Free ion pair	% M-SO_4 pair	% M-HCO_3^- pair	% M-CO_3^{2-} pair	% M-Cl^- pair
Ca^{2+}	3.95×10^{-4}	98.33	1.00	0.65	0.01	—
Mg^{2+}	3.65×10^{-4}	98.22	1.18	0.60	0.01	—
Fe^{2+}	2.26×10^{-4}	91.87	0.83	4.78	2.51	—
Mn^{2+}	1.31×10^{-5}	94.13	0.86	4.37	0.65	—
Na^+	1.94×10^{-3}	99.93	0.03	0.03	—	—
K^+	2.95×10^{-4}	99.95	0.05	—	—	—

Ion	Molality (Total) moles kg^{-1}	% Free ion	% Ca-X pair	% Mg-X pair	% Fe-X pair	% Mn-X pair	% Na-X pair	% K-X pair
SO_4^{2-}	1.05×10^{-4}	90.23	3.77	4.09	1.79	0.11	—	—
HCO_3^-	7.25×10^{-4}	97.77	0.36	0.30	1.49	0.08	—	—
CO_3^{2-}	6.00×10^{-6}	2.67	0.94	0.49	94.48	1.41	—	—

ionic strength and the ion activity coefficients for the various dissolved species are again determined. The next step is to determine whether or not the water as a result of a pH change has become saturated with respect to any of the solid phases considered. To determine the degree of saturation, the ion activity products (IAP) are computed for each phase and compared with the equilibrium values. If the IAP for a particular mineral exceeds its equilibrium value, then the water is supersaturated with respect to that mineral, and precipitation of the phase is assumed to commence. However, once a particular solid starts precipitating, because its IAP remains constant, thereafter, the phase also becomes a pH-dependent species, and the molality of the cation of that species can be expressed as a negative term on the left side of the electrical neutrality eq (9). For instance, if at a particular concentration the water is saturated with, say siderite, we can write the new charge balance equation as

$$\frac{10^{-11.32}}{\gamma_{HCO_3^-} a_{H^+}} + \frac{2(10^{-21.649})}{(\gamma_{CO_3^{2-}} a_{H^+}^2)} + \frac{10^{-14}}{\gamma_{OH^-} a_{H^+}} - \frac{a_{H^+}}{\gamma_{H^+}} - 2m_{Fe^{2+}} =$$

$$2m_{Ca^{2+}} + 2m_{Mg^{2+}} + 2m_{Mn^{2+}} + m_{Na^+} + m_{K^+} - 2m_{SO_4^{2-}} - m_{Cl^-} \quad (10)$$

For the equation

$$FeCO_{3(s)} = Fe^{2+}_{(aq)} + CO^{2-}_{3(aq)},$$

$$K_{sp} = a_{Fe^{2+}} a_{CO_3^{2-}} = 10^{-10.80} \quad \text{(from Table 3)} \quad (10.1)$$

$$a_{Fe^{2+}} = \frac{10^{-10.80}}{a_{CO_3^{2-}}} \tag{10.2}$$

$$m_{Fe^{2+}} = \frac{10^{-10.80}}{\gamma_{Fe^{2+}} a_{CO_3^{2-}}} \tag{10.3}$$

We know

$$m_{CO_3^{2-}} = \frac{2(10^{-21.649})}{(\gamma_{CO_3^{2-}} a_{H^+}^2)} \quad \text{(from eq 6)}$$

Substituting for $a_{CO_3^{2-}}$ we obtain

$$m_{Fe^{2+}} = \frac{10^{-10.80} a_{H^+}^2}{10^{-21.649} \gamma_{Fe^{2+}}} \tag{10.4}$$

Substituting for $m_{Fe^{2+}}$ in eq (10), the expression can be solved by the iterative method outlined to obtain the pH of water in equilibrium with siderite and atmospheric P_{CO_2}. The final analytical expression after the water is saturated with all the solids considered is

$$m_{Na^+} + m_{K^+} + 2m_{SO_4^{2-}} - m_{Cl^-} = \frac{10^{-11.32}}{\gamma_{HCO_3^-} a_{H^+}} + \frac{2(10^{-21.649})}{\gamma_{CO_3^{2-}} a_{H^+}^2} + \frac{10^{-14}}{\gamma_{OH^-} a_{H^+}} - \frac{a_{H^+}}{\gamma_{H^+}} - \frac{2a_{H^+}^2}{\gamma_{Fe^{2+}} 10^{-10.85}} - \frac{2a_{H^+}^2}{\gamma_{Mn^{2+}} 10^{-11.07}} - \frac{2a_{H^+}^2}{\gamma_{Ca^{2+}} 10^{-13.19}} - \frac{2a_{H^+}^2}{\gamma_{Mg^{2+}} 10^{-13.63}} \tag{11}$$

The calculated changes in water composition during evaporation up to 1000× concentration and the various solids precipitating out at different concentration levels are shown in figure 7. Figure 8 shows the ionic strength and the pH of the water corresponding to various evaporative concentrations.

Sensitivity analysis.—Because the formation and stability of siderite necessitates a very narrow range of redox conditions (see fig. 1, for instance), endogenic precipitation of this iron-carbonate phase is very sensitive to inputs and variations in the chemistry of the depositional waters. In particular, our model is based on the critical assumption that an oxic freshwater aqueous system, maintaining an adequate supply of reactive iron in the reduced state, can become supersaturated as it is allowed to evaporate isothermally at 25°C in equilibrium with atmospheric CO_2. In order to assess the response of such a system to changes in the initial dissolved concentrations of iron and bicarbonate, as well as the effects of organic complexation, a sensitivity analysis of the model was

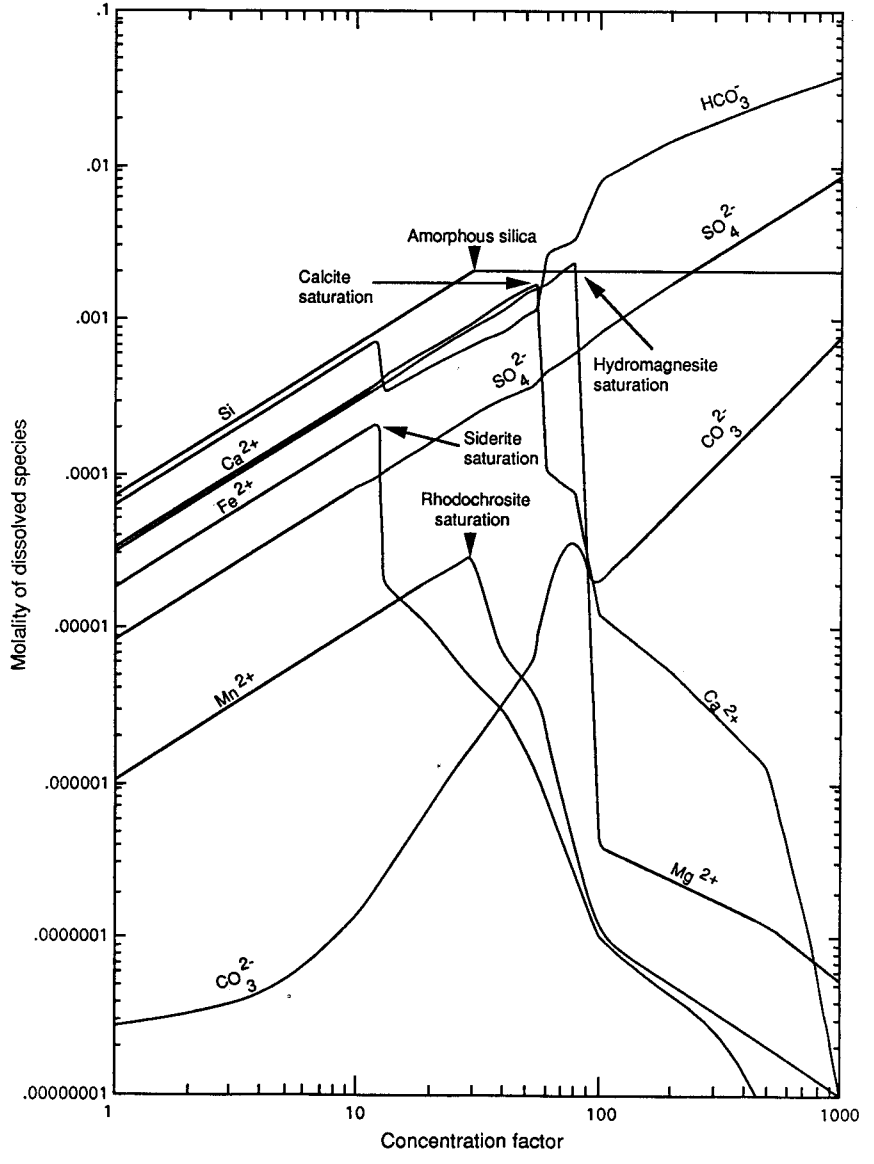

Fig. 7. Calculated results of evaporation of Satilla drainage water at 25°C in equilibrium with atmospheric P_{CO_2} of $10^{-3.5}$ atm.

performed by varying the concentrations of these components in our calculations. As indicated earlier, we assumed that the initial HCO_3^- concentration of the Black Sea feedwater was equal to 4.1 ppm (compared with a reported average value of 2.6 ppm for the Satilla drainage),

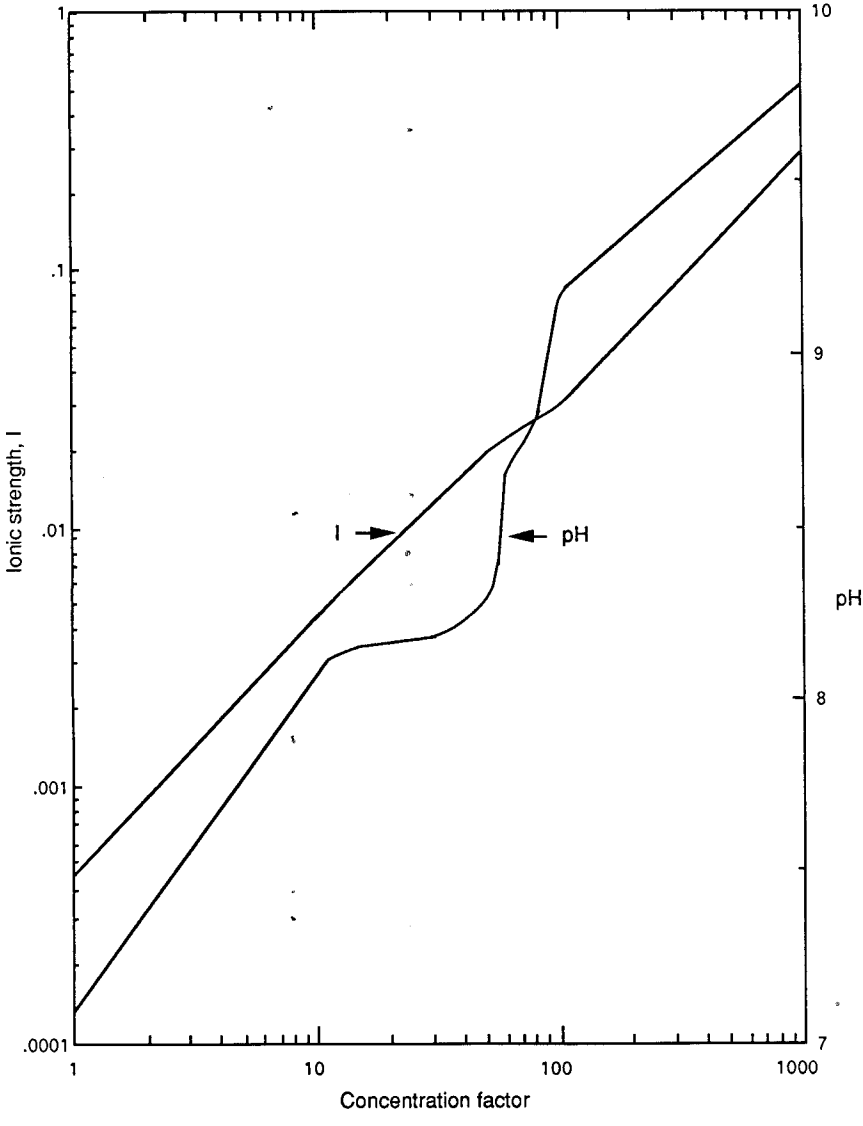

Fig. 8. Calculated ionic strength and pH of the feedwater at different evaporative concentrations.

a value that corresponds to the average bicarbonate concentration of Satilla water in its upper reaches. Our calculations resulting from the sensitivity analysis show that even for an initial HCO_3^- concentration of 2.6 ppm, for the assumed concentration of iron, siderite is the earliest

carbonate phase to precipitate (at about 14× concentration of the waters, followed by rhodochrosite at about 32×). We also performed the calculations by assuming that only a third of the total analytical iron concentration in the waters reaching the depositional basin is available as free Fe^{2+} and by correcting the initial electrical imbalance by considering dissociated carboxylate anions in the charge balance. Even under such constraints, siderite turns out to be first carbonate phase to reach saturation, at an evaporative concentration of the waters to 15×. The presence of organic anions as an independent component thus does not significantly alter our model results, at least within the range of evaporative concentrations leading to siderite saturation. Similarly, if a feedwater containing only 2.6 ppm of HCO_3^- and 0.35 ppm of uncomplexed Fe^{2+} (equal to a third of the original analytical concentration of iron in the Satilla river system) is allowed to evaporate in equilibrium with atmospheric CO_2, the water becomes saturated with respect to siderite first, although only at a higher evaporative concentration of ~25×. In fact, the calculations show that the separation between the evaporative concentrations at which the various carbonate phases reach saturation only increases under these varying conditions of solution composition.

Composition of Carbonates

Three distinct solid carbonate phases were considered: pure calcite, $CaCO_3$; a complete and ideal solid solution between siderite ($FeCO_3$) and rhodochrosite ($MnCO_3$); and an ideal, complete solid solution between ankerite ($Fe_{0.5}Ca_{0.5}CO_3$) and kutnahorite ($Mn_{0.5}Ca_{0.5}CO_3$). The two solid solutions can be represented, respectively, by the following formulae

$$Fe_{X_{sid}}Mn_{(1-X_{sid})}CO_3$$

and

$$Fe_{0.5X_{ank}}Mn_{0.5(1-X_{ank})}Ca_{0.5}CO_3$$

where X_{ank} and X_{sid} represent the mole fractions of the endmembers ankerite and siderite, respectively. Considering calcite as a pure phase (activity = 1) and assuming the solid solutions to be ideal (activity of the solid = mole fraction), the following mass action equations can be written

$$K_c = a_{Ca^{2+}}a_{CO_3^{2-}} \tag{12}$$

$$K_s = \frac{a_{Fe^{2+}}a_{CO_3^{2-}}}{X_{Sid}} \tag{13}$$

$$K_r = \frac{a_{Mn^{2+}}a_{CO_3^{2-}}}{(1 - X_{sid})} \tag{14}$$

$$K_a = \frac{(a_{Fe^{2+}})^{0.5}(a_{Ca^{2+}})^{0.5}(a_{CO_3^{2-}})}{X_{ank}} \tag{15}$$

$$K_k = \frac{(a_{Mn^{2+}})^{0.5}(a_{Ca^{2+}})^{0.5}(a_{CO_3^{2-}})}{1 - X_{ank}} \tag{16}$$

where K_c, K_s, K_r, K_a, and K_k are, respectively, the equilibrium constants for pure calcite, siderite, rhodochrosite, ankerite, and kutnahorite at 25°C and 1 atm (table 3).

The composition of each solid solution is fixed by the ratio of Fe^{2+} to Mn^{2+} in solution, as shown by the following equations

$$\frac{K_s}{K_r} = \frac{a_{Fe^{2+}}(1 - X_{sid})}{a_{Mn^{2+}}X_{sid}} \tag{17}$$

$$\frac{K_a^2}{K_k^2} = \frac{a_{Fe^{2+}}(1 - X_{ank})^2}{a_{Mn^{2+}}(X_{ank})^2} \tag{18}$$

The two solid solutions may coexist with an aqueous phase of a given $a_{Fe^{2+}}/a_{Mn^{2+}}$ ratio. Their respective compositions are fixed by the following relation, obtained by combining eqs (17) and (18)

$$\frac{X_{sid}K_s}{(1 - X_{sid})K_r} = \left(\frac{(X_{ank}K_a)}{(1 - X_{ank})K_k}\right)^2 \tag{19}$$

The relations between the solid phases and aqueous solution can be best represented by a solid solution-aqueous solution phase diagram for the system CaO–MnO–FeO–CO_2–H_2O system (Helgeson, 1968; Helgeson, Garrels, and Mackenzie, 1969; Woods and Garrels, 1992). It can be shown that the stability of the various solid phases can be described in terms of the two variables $a_{Fe^{2+}}/a_{Ca^{2+}}$ and $a_{Mn^{2+}}/a_{Ca^{2+}}$. Let us first consider the boundary in the calcite-ankerite-kutnahorite system. By dividing eqs (15) and (16) by eq (12), one obtains the following expressions for the equilibrium between calcite and an ankerite-kutnahorite solid solution

$$\frac{X_{ank}^2K_a^2}{K_c^2} = \frac{a_{Fe^{2+}}}{a_{Ca^{2+}}} \tag{20}$$

$$\frac{(1 - X_{ank})^2K_k^2}{K_c^2} = \frac{a_{Mn^{2+}}}{a_{Ca^{2+}}} \tag{21}$$

For each composition of the solid solution, given by X_{ank}, there is only one fixed value for each of the ratios $a_{Fe^{2+}}/a_{Ca^{2+}}$ and $a_{Mn^{2+}}/a_{Ca^{2+}}$. This condition can be represented in a log $a_{Fe^{2+}}/a_{Ca^{2+}}$ − log $a_{Mn^{2+}}/a_{Ca^{2+}}$ orthogonal composition diagram (fig. 9). The calculated curve, obtained by using the data of table 3, delineates the stability field of calcite with respect to the ankerite-kutnahorite solid solution. The two solid phases may only coexist for a composition of the aqueous phase represented by one point on the curve. The coexistence of the ankerite-kutnahorite solid

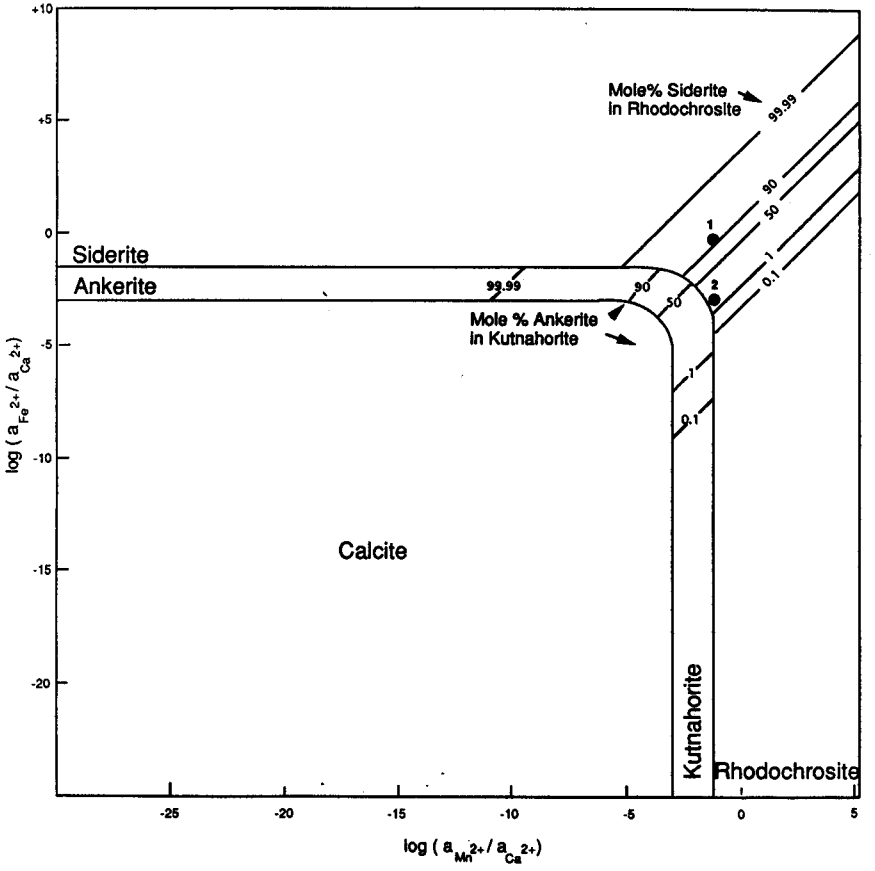

Fig. 9. Aqueous solution-solid solution phase diagram for the system CaO–FeO–MnO–CO_2–H_2O at 25°C and 1 atm. total pressure. The stability fields of the various carbonate phases and solid solutions are indicated. The compositions of the solid solutions, siderite-rhodochrosite, and ankerite-kutnahorite, in equilibrium with an aqueous solution are also shown. Points 1 and 2 represent the compositions of the solid solution in equilibrium with water for an evaporative concentration of 12× and 35×, respectively.

solution with the siderite-rhodochrosite solid solution can be obtained in a similar way by combining relations (13) and (14), respectively, with the square of (15) and (16)

$$\frac{X_{sid}^2 K_s^2}{X_{ank}^2 K_a^2} = \frac{a_{Fe^{2+}}}{a_{Ca^{2+}}} \tag{22}$$

$$\frac{(1 - X_{sid})^2 K_r^2}{(1 - X_{ank})^2 K_k^2} = \frac{a_{Mn^{2+}}}{a_{Ca^{2+}}} \tag{23}$$

The two coexisting solid solutions must furthermore fulfill the following condition

$$\frac{X_{sid}K_s}{(1 - X_{sid})K_r} = \left(\frac{(X_{ank}K_a)}{(1 - X_{ank})K_k}\right)^2 \quad (24)$$

Thus, by combining eqs (24), (22), and (23), one obtains once more for each composition of the solid solution, a fixed value for the ratios $a_{Fe^{2+}}/a_{Ca^{2+}}$ and $a_{Mn^{2+}}/a_{Ca^{2+}}$. The results are represented in the log-log diagram (fig. 9) as before.

The composition of the solid solutions in equilibrium with an aqueous solution can also be represented in figure 9, in the manner as described above. The equilibrium conditions for siderite-rhodochrosite given by relation (17) are rewritten as

$$\log \frac{a_{Fe^{2+}}}{a_{Ca^{2+}}} = \log \frac{X_{sid}K_s}{(1 - X_{sid})K_r} + \log \frac{a_{Mn^{2+}}}{a_{Ca^{2+}}} \quad (25)$$

Each composition of the solid solution X_{sid} is described in the diagram by a straight line of slope 1. Similarly, the equilibrium condition (18) for the ankerite-kutnahorite solid solution is

$$\log \frac{a_{Fe^{2+}}}{a_{Ca^{2+}}} = 2 \log \left(\frac{(X_{ank}K_a)}{(1 - X_{ank})K_k}\right) + \log \frac{a_{Mn^{2+}}}{a_{Ca^{2+}}} \quad (26)$$

This condition is also represented by a straight line of slope 1 for each value of X_{ank}.

DISCUSSION

The changes in water composition during evaporation up to 1000× and the various solids precipitating out at different evaporative concentration levels are shown in figures 7 and 8. The first solid phase to precipitate out of this water is siderite, at a concentration of about 12×. Increasing the degree of evaporative concentration and precipitation of siderite will gradually change the $a_{Fe^{2+}}/a_{Mn^{2+}}$ ratio in favor of saturation of the solution with respect to rhodochrosite. By the time saturation with respect to rhodochrosite is attained (at about 35×), most of the free ferrous iron in solution is removed as the carbonate phase. The composition of the iron-manganese carbonate phase in equilibrium with the aqueous solution for different evaporative concentrations can be determined by plotting the log $a_{Mn^{2+}}/a_{Ca^{2+}}$ against log $a_{Fe^{2+}}/a_{Ca^{2+}}$ on the equilibrium phase diagram of figure 9. Thus, an evaporative concentration of 12× would yield a nearly pure siderite, while for a 35× concentration of the waters, pure rhodochrosite will result. At evaporative concentrations between 12× and 35×, the composition of the mixed Fe-Mn carbonate phase in equilibrium with the aqueous medium will be a function of the $a_{Fe^{2+}}/a_{Mn^{2+}}$ ratio in solution. The waters at a concentration of about 55× are saturated with respect to calcite, while precipitation

of hydromagnesite does not start until the concentration is around 75× (fig. 7).

A few comments on the role of silica in this evaporation model are appropriate here. It is difficult to postulate the role of abiotic processes in extracting dissolved silica from the surface waters of the Black Sea basin, although it has been suggested that sorption reactions involving dissolved silica and suspended sediments are a likely buffering mechanism in controlling silica concentrations in fresh water environments (Edwards and Liss, 1973; Mayer and Gloss, 1980). Diatoms constitute nearly 50 to 60 percent of the bulk of the two siderite units in the Black Sea section (Ross, 1978). Such an abundance of diatoms indicates that the silica cycle of the Neogene Black Sea was principally driven by biologic activity. It is quite likely, therefore, that biotic uptake had always maintained silica concentration in the Black Sea waters below the saturation concentration for inorganic precipitation of this component, either as amorphous silica or as the Mg-silicate phase, sepiolite (Wollast, Mackenzie, and Bricker, 1968).

A critical aspect of this model is our assumption of equilibrium between the precipitating iron carbonate phase and the depositional waters. Equilibrium thermodynamics, despite its limitations when applied to natural mineral-water systems, does provide strong constraints on the behavior of natural systems. As we noted earlier, the siderites in the Black Sea, present as finely disseminated grains or confined to finely laminated horizons, are remarkably uniform in their morphology and textural characteristics. Quantitative electron microprobe analyses do not show any noticeable variation in composition within individual siderite grains. Furthermore, there are no indications of the formation of these carbonate phases by recrystallization from metastable phases. Thus we contend that the siderites in the Plio-Pleistocene Black Sea sedimentary record are the ones initially deposited in equilibrium with the depositional waters. Although such situations may be a rarity in near-surface aquatic systems, equilibrium between authigenic carbonates and the aqueous phase has been demonstrated in several aquifer systems, for example, in the lower Rhine valley near Bocholt in Germany (Leuchs and Obermann, 1992) and in the Coastal Plain aquifers of the southeastern United States (Lee, 1985; Lee and Strickland, 1988). Similarly, Anthony (1977) has reported the formation of siderite in the water column of the modern freshwater Lake of the Clouds, Minnesota (1977).

How does this evaporative model explain the siderite occurrences in the Black Sea? Basically, the model establishes that in an oxic freshwater aquatic system capable of maintaining relatively high concentrations of Fe^{2+} in the presence of suitable organic ligands, it is theoretically possible for siderite to precipitate, by a simple process of evaporative concentration, much before the waters saturate with respect to any other carbonate phase. However, the persistence of siderite in the sediments is subject to the various thermodynamic constraints enumerated earlier (see fig. 1). What we emphasize in our model is the possibility of water column

precipitation of siderite grains in a depositional basin receiving waters of a suitable composition. The process of precipitation is controlled by the evaporative concentration of the entire water mass, while the preservation of this carbonate phase in the sediment record is due to the existence of at least periodically stagnant, anoxic bottom waters (as discussed earlier). The model also provides for the formation of discrete layers or laminae of the siderite phase alone, if detrital flux into the basin is largely excluded. Depending on the extent of terrigenous dilution, endogenic siderite can also occur as disseminations, admixed with clastics.

Combining the theoretical model results with the climatostratigraphic and paleoenvironmental constraints enables a reconstruction of the history of siderite sedimentation and water balance for the Plio-Pleistocene Black Sea. As discussed earlier, closed basin lacustrine conditions persisted in the Black Sea during most of the times of deposition of the sideritic units. Hence because there was practically no water exchange with the Mediterranean during these periods, the oligohaline to mesohaline conditions postulated for the Black Sea by Schrader (1978) would imply a salinization of the waters by evaporitic excesses. Our model results indicate that if the Black Sea feed water during the times of siderite deposition had a composition similar to present-day Satilla drainage, an evaporative concentration of the water of the order of about 12× is sufficient to initiate siderite precipitation.

Climatostratigraphical interpretations of the Caspian–Black Sea–Mediterranean system and palynological studies of the Black Sea sediment cores indicate that warm, humid climatic conditions prevailed in the Black Sea catchment areas during most of the times of siderite deposition (Traverse, 1978; Hsü, 1978; this study). This could have led to intense chemical weathering of the hinterland lithologies, yielding abundant fluvial inputs of iron associated with humic substances to the depositional basin. The dominance of ^{12}C-enriched organic matter in the sediments ($\delta^{13}C$ of bulk organic matter ranges between −24.9 and −27.7 permil; study in progress), its relatively high C/N ratio (mean C/N ratio 11), and low H/C ratio (<1.0 in the lower Siderite unit; Huc, Durand and Monin, 1978) corroborate our hypothesis of a higher flux of terrigenous organic matter into the basin during the times of siderite deposition.

The present-day Black Sea is marked by 550 $km^3\ y^{-1}$ of fresh water inflow through runoff and precipitation, and an evaporation rate of 350 $km^3\ y^{-1}$. Nearly 50 percent of the *total* water influx into the basin is lost through evaporation. If deprived of the two-way flow through the Bosporus, the water balance of the Black Sea during the times of siderite deposition must have been quite different from that of the present day. Our paleoenvironmental interpretations based on climatostratigraphy indicate that climatic conditions were relatively warmer and more humid and temperature gradients between summer and winter were steeper during the times of siderite deposition than they are today. Under these conditions, fresh water inflow must also have increased to offset the

increased evaporation. Such a change in the hydrological regimen of the Black Sea seems comparable to the development of brackish water in the Caspian basin during the late Khazar regression ($>70 \times 10^3$ ybp). Chepalyga (1984) estimated that the warm, humid climatic conditions that prevailed in the drainage basin of the arid Caspian region during this time led to a 33 percent increase in runoff and a 20 percent increase in the loss due to evaporation, relative to present-day values.

Palynological evidence from southern Italy, Sicily, and southwestern France points to the existence of latitudinal gradients in vegetation, and hence in climate, within the Mediterranean region during Pliocene-early Pleistocene times (Suc, 1984; Bertoldi, Rio, and Thunell, 1989; Thunell and others, 1991). For instance, while pollen records for the Early Pliocene from southern Italy and Sicily indicate the prevalence of an arid climate with dry summers in the south-central Mediterranean region during the Early Pliocene, the flora of the northwestern Mediterranean suggests warm humid climatic conditions during this time period (Bertoldi, Rio, and Thunell, 1989). Similarly, the vegetational record corresponding to the short-term climatic cooling centered at around 3.2 Ma for these two regions is characteristically different. While the climatic conditions in the southwestern Mediterranean were relatively cool and more humid during this time, arid conditions prevailed in the northwest. Thus, we contend that the existence of contrasting climatic regimes in the catchment areas and the basin proper of the Plio-Pleistocene Black Sea as necessitated by our model is not in conflict with the climatic conditions that prevailed in much of western Europe during this time span.

If disseminations of siderite crystals in sediments can be explained by a simple process of evaporation, can the interlayers and interbeds of siderite-rich horizons in the Black Sea record result from this process? To answer this question, we calculated the thickness of pure siderite deposited in one year per cm^2 of the basin for an evaporative concentration of 12×, as follows: The difference in the concentration of Fe^{2+} at 12× and the next higher concentration (13×) is equivalent to the amount of Fe^{2+} removed from solution as siderite. This amount (in mg l^{-1}) was converted to milligrams of iron deposited per cm^2 of basin area. Considering the density of siderite to be 3.80 g cm^{-3}, the milligrams of iron deposited per cm^2 of area were recalculated to millimeters per cm^2 of siderite precipitated in the basin. If the evaporative concentration (by a factor of 12×) and precipitation of siderite are an annual process, then, our calculations indicate that the thickness of pure siderite that will be precipitated per year from a liter of basin water is only 0.06 mm. Therefore, a 10 cm layer of pure siderite would require more than 1700 years to precipitate! The values will not change much even for higher evaporative concentrations where the water is saturated with respect to other carbonate phases as well (see fig. 7). Hsü and Giovanoli (1979) have estimated a sedimentation rate of 0.18 mm per yr for the two siderite-rich sequences. If this value represents the rate at which terrigenous/diatomaceous clays were deposited in the basin, evaporative concentra-

tion and settling out of siderite grains at a much lower rate will result in disseminations of this carbonate phase in the clay sequence, as observed. At these rates of sedimentation, the thicker, centimeter-to decimeter-scale interbeds and interlayers of siderite can only be diagenetic horizons or a composite of many microlayers of pure or Fe–Mn–Ca siderite precipitated from the water column.

CONCLUSIONS

A major conclusion derived from the present study is that endogenic siderites are a distinct possibility in fresh water lacustrine environments marked by annual productivity cycles, thermal stratification, anoxic bottom waters, and an adequate supply of iron. The nature and composition of the sideritic phase that can precipitate out are a function of the evaporitic concentration of water, and its persistence in the sediment record is constrained by several thermodynamic variables including low pe and concentration of dissolved sulfide, high P_{CO_2}, and availability of organic matter. The application of our model to the geological history of sedimentation in the Black Sea indicates that climate was the chief forcing function in transforming the calcite-precipitating eutrophic water masses of the basin into one of siderite precipitation during interludes in the basin's Plio-Pleistocene history. Based on calculations of the thickness of siderite precipitated per cm^2 of basin area, we further predict the presence of microlaminations in the observed interlayers and interbeds of sideritic mud. It is also interesting to note that the occurrence of siderite in the Black Sea, ranging from microbands to interlayers and interbeds is remarkably similar to the Early Proterozoic Hamersley Banded Iron Formations, whose striking textural similarity with the Permian Castile carbonate-anhydrite varves prompted Garrels (1987) to develop an evaporative model for the Banded Iron Formation microbands.

ACKNOWLEDGMENTS

We wish to thank the Ocean Drilling Program for supplying samples. We are grateful to Bob Berner (Yale), Ken Hsü (ETH-Zürich), John Morse (Texas A&M), and an anonymous reviewer, who reviewed earlier versions of this manuscript and offered many constructive suggestions. Travel to collect the samples and initial funds for isotopic analyses were provided to CRG by the Swiss Federal Institute of Technology (ETH) while on leave from UH. Acknowledgment is made to the Donors of The Petroleum Research Fund, administered by the American Chemical Society, for support of this research (ACS-PRF # 27446-AC8 to CRG). FTM's contribution was supported by EAR93-16133. This is UH SOEST contribution number 4065.

References

Aharon, P., 1988, A stable isotopic study of magnesites from the Rum Jungle Uranium Field, Australia: implications for the origin of stratabound massive magnesites: Chemical Geology, v. 69, p. 127–145.

Anthony, R. S., 1977, Iron-rich rhythmically laminated sediments in Lake of the Clouds, northeastern Minnesota: Limnology and Occanography, v. 22, p. 45–54.

Arnold, R. G., Di Christina, T. J., and Hoffmann, M. R., 1988, Dissimilative Fe (III) reduction by *Pseudomonas* sp 200—inhibition studies: Applied Environmental Microbiology, v. 52, p. 281–294.

Bahrig, B., 1988, Paleoenvironment information from deep water siderite (Lake of Laach, West Germany), *in* Fleet, A. J., Kelts, K., and Talbot, M. R., editors, Lacustrine Petroleum Source Rocks, Geological Society of London Special Publication no. 40: Oxford, Blackwell Scientific, p. 153–158.

———— 1989, Stable isotope composition of siderite as an indicator of the paleoenvironmental history of oil shale lakes: Palaeogeography, Paleoclimatology, Palaeoccology, v. 70, p. 139–151.

Balkas, T., Dechev, G., Mihnea, R., Serbanescu, O., and Unluata, U., 1990, State of the marine environment in the Black Sea region: UNEP Regional Seas Reports and Studies, 124, p. 1–13.

Beck, K. C., Reuter, J. H., and Perdue, E. M., 1974, Organic and inorganic geochemistry of some coastal plain rivers of the southeastern United States: Geochimica et Cosmochimica Acta, v. 38, p. 341–364.

Bernard, A., and Symonds, R. B., 1989, The significance of siderite in the sediments from Lake Nyos, Cameroon: Journal of Volcanology and Geothermal Research, v. 39, p. 187–194.

Berner, R. A., 1981, A new geochemical classification of sedimentary environments: Journal of Sedimentary Petrology, v. 51, p. 359–365.

Bertoldi, R., Rio, D., and Thunell, R., 1989, Pliocene-Pleistocene vegetational and climatic evolution of the South-Central Mediterranean: Palaeogeography, Palaeoclimatology, Palaeoecology, v. 72, p. 263–275.

Beukes, N. J., and Klein, C., 1992, Models for iron-formation deposition, *in* Schopf, J. W., and Klein, C., editors, The Proterozoic Biosphere: A Multidisciplinary Study: Cambridge, United Kingdom Cambridge University Press, p. 147–151.

Beukes, N. J., Klein, C., Kaufman, A. J., and Hayes, J. M., 1990, Carbonate petrography, kerogen distribution, and carbon and oxygen isotope variations in an early Proterozoic transition from limestone to iron-formation deposition, Transvaal Supergroup, South Africa: Economic Geology, v. 85, p. 663–690.

Bruno, J., Wersin, P., and Stumm, W., 1992, On the influence of carbonate in mineral dissolution. II. The stability of FeCO3(s) at 25°C and 1 atm. total pressure: Geochemica et Cosmochemica Acta, v. 56, p. 1149–1155.

Burton, E., Machel, H. G., and Qi, J., 1993, Thermodynamic constraints on anomalous magnetization in shallow and deep hydrocarbon seepage environments: Society of Economic Paleontologists and Mineralogists Special Publication, 49, p. 193–207.

Carothers, W. W., Adami, L. H., and Rosenbauer, R. J., 1988, Experimental oxygen isotope fractionation between siderite-water and phosphoric acid liberated CO_2-siderite: Geochemica et Cosmochemica Acta, v. 52, p. 2445–2450.

Chepalyga, A. L., 1984, Inland sea basins, *in* Velichko, A. A., editor, Late Quaternary Environments of the Soviet Union: Minneapolis, University of Minnessotta Press, p. 229–247.

Cole, J. J., Caraco, N. F., Kling, G. W., and Kratz, T. K., 1994, Carbon dioxide supersaturation in the surface waters of lakes: Science, v. 265, p. 1568–1570.

Coleman, M. L., 1985, Geochemistry of diagenetic non-silicate minerals: Kinetic considerations: Philosophical Transactions of the Royal Society of London, (A), v. 315, p. 39–56.

Cortecci, G., and Frizzo, P., 1993, Origin of siderite deposits from the Lombardy Valleys, northern Italy: a carbon, oxygen and strontium isotope study: Chemical Geology, v. 105, p. 293–303.

Curtis, C. D., 1967, Diagenetic iron minerals in some British Carboniferous sediments: Geochemica et Cosmochemica Acta, v. 31, p. 2109–2123.

———— 1977, Sedimentary geochemistry: Environments and processes dominated by involvement of an aqueous phase: Philosophical Transactions of the Royal Society of London, (A), v. 286, p. 353–372.

Curtis, C. D., 1987, Mineralogical consequences of organic matter degradation in sediments: Inorganic/organic diagenesis, *in* Leggett, J. K., and Zutta, G. G., editors, Marine Clastic Sedimentology: London, Graham & Trotman, p. 108–123.
Curtis, C. D., and Spears, D. A., 1968, The formation of sedimentary iron minerals: Economic Geology, v. 63, p. 257–270.
Dahm, H. D., 1956, Diatomeenuntersuchungen zur Geschichte der westlichen Ostsee: Meyniana, v. 5, p. 7–50.
Davison, W., 1993, Iron and manganese in lakes: Earth-Science Reviews, v. 34, p. 119–163.
Degens, E. T., and Paluska, A., 1979, Tectonic and climatic pulses recorded in Quaternary sediments of the Black Sea region: Sedimentary Geology, v. 23, p. 149–163.
Degens, E. T., and Ross, D. A., editors, 1974, The Black Sea—Geology, Chemistry, and Biology: American Association of Petroleum Geologists Memoir 20, 633 p.
Deuser, W. G., Degens, E. T., and Stoffers, P., 1978, O^{18} and C^{13} contents of carbonates from Deep Sea Drilling Sites in the Black Sea, *in* Ross, D. A., Neprochnov, Y. P., et al., editors, Initial Reports of the Deep Sea Drilling Project, v. 42, Part 2: Washington, D. C., United States Government Printing Office, p. 617–623.
Edwards, A. M. C., and Liss, P. S., 1973, Evidence for buffering of dissolved silicon in fresh waters: Nature, v. 243, p. 341–342.
Emelyanov, E. M., Lisitzin, A. P., Shimkus, K. M., Trimonis, E. S., Lukashev, V. K., Lukashin, V. K., Mitropolskiy, A. Yu., Pilipchuk, M. F., Shirshov, P. P., 1978, Geochemistry of late Cenozoic sediments of the Black Sea, Leg 42, v. 42, Part 2: Washington, D.C., United States Government Printing Office, p. 543–605.
Fonselius, S. N., 1974, Phosphorus in Black Sea, *in* Degens, E. T., and Ross, D. A., editors, The Black Sea—Geology, Chemistry, and Biology: American Association of Petroleum Geologists Memoir 20, p. 144–150.
Fritz, P., Binda, P. L., Folinsbee, F. E., and Krouse, H. R., 1971, Isotopic composition of diagenetic siderites from Cretaceous sediments in western Canada: Journal of Sedimentary Petrology, v. 41, p. 282–288.
Froelich, P. N., Klinkhammer, G. P., Bender, M. L., Luedtke, N. A., Heath, G. R., Cullen, D., Dauphin, P., Hammond, D., Hartman, B., and Maynard, V., 1979, Early oxidation of organic matter in pelagic sediments of the equatorial Atlantic: suboxic diagenesis: Geochimica et Cosmochimica Acta, v. 43, p. 1075–1090.
Garrels, R. M., 1987, A model for the deposition of the microbanded Precambrian iron formations: American Journal of Science, v. 287, p. 81–106.
———— 1988, Reply—A model for the deposition of the microbanded Precambrian Iron Formations: American Journal of Science, v. 288, p. 669–673.
Garrels, R. M., and Christ, C. L., 1965, Solutions, Minerals, and Equilibria: San Francisco, Freeman, Cooper & Company, 450 p.
Garrels, R. M., and Mackenzie, F. T., 1967, Origin of the chemical compositions of some springs and lakes, *in* Equilibrium Concepts in Natural Water Systems: American Chemical Society, Advances in Chemistry Series v. 67, p. 222–242.
———— 1971, Evolution of Sedimentary Rocks: New York, W. W. Norton and Co., 397 p.
———— 1972, A quantitative model for the sedimentary rock cycle: Marine Chemistry, v. 1, p. 22–41.
Garrels, R. M., and Thompson, M. E., 1962, A chemical model for sea water at 25°C and one atmosphere total pressure: American Journal of Science, v. 260, p. 57–66.
Gautier, D. L., 1982, Siderite concretions: indicators of early diagenesis in the Gammon Shale (Cretaceous): Journal of Sedimentary Petrology, v. 52, p. 859–871.
Ghosh, M. M., O'Connor, J. T., and Engelbrecht, R. S., 1967, Bathophenanthroline method for the determination of ferrous iron: Journal of American Water Works Association, v. 59, p. 897–905.
Glenn, C. R., and Arthur, M. A., 1990, Anatomy and origin of a Cretaceous phosphorite-greensand giant, Egypt: Sedimentology, v. 37, p. 123–154.
Glenn, C. R., Rajan, S., Hsü, K. J., and Popp, B. N., 1992, Cyclic sedimentation, paleoclimate and paleoceanography of the Plio-Pleistocene Black Sea: International Geological Congress, 29th, Kyoto, Japan, Abstracts, v. 2, p. 287.
Golyshev, S. I., Padalko, N. L., and Pechenkin, S. A., 1981, Fractionation of stable oxygen and carbon isotopes in carbonate systems: Geokhimiya, v. 10, p. 1427–1441.
Hardie, L. A., and Eugster, H. P., 1970, The evolution of closed-basin brines: Mineralogical Society of America Special Paper, v. 3, p. 273–290.
Harland, W. B., Armstrong, R. L., Cox, A. V., Craig, L. E., Smith, A. G., and Smith, D. G., 1990, A Geologic Time Scale, 1989: Cambridge, United Kingdom, Cambridge University Press, 263 p.

Helgeson, H. C., 1968, Evaluation of irreversible reactions in geochemical processes involving minerals and aqueous solutions—I. Themodynamic relations: Geochimica et Cosmochimica Acta, v. 32, p. 853–877.
Helgeson, H. C., Delaney, J. M., Nesbitt, W. H., and Bird, D. K., 1978, Summary and critique of the thermodynamic properties of rock-forming minerals: American Journal of Science, v. 278A, p. 44–51.
Helgeson, H. C., Garrels, R. M., and Mackenzie, F. T., 1969, Evaluation of irreversible reactions in geochemical processes involving minerals and aqueous solutions—II. Applications: Geochimica et Cosmochimica Acta, v. 33, p. 455–481.
Hering, J. G., and Stumm, W., 1990, Oxidative and reductive dissolution of minerals, *in* Hochella, M. F., and White, A. F., editors, Mineral-Water Interface Geochemistry: Mineralogical Society of America, Reviews in Mineralogy; v. 23, p. 427–465.
Hsü, K. J., 1978a, Stratigraphy of the lacustrine sedimentation in the Black Sea, *in* Ross, D. A., Neprochnov, Y. P., and others, editors, Initial Reports of the Deep Sea Drilling Project, v. 42, Part 2: Washington, United States Government Printing Office, p. 509–524.
———— 1978b, When the Black Sea was drained: Scientific American, v. 238, p. 53–63.
Hsü, K. J., and Giovanoli, F., 1979, Messian event in the Black Sea: Palaeogeography, Palaeoclimatology, Palaeoccology, v. 29, p. 75–93.
Hsü, K. J., and Kelts, K., 1978, Late Neogene chemical sediments in the Black Sea, *in* Matter, A., and Tucker, M. E., editors, Modern and Ancient Lake Sediments: International Association of Sedimentologists, Special Publications v. 2: Oxford, Blackwell, p. 129–145.
Hue, A. Y., Durand, B., Monin, J. C., 1978, Humic compounds and kerogens in cores from Black Sea sediments, Leg 42B—Holes 379A, B, and 380A, *in* Ross, D. A., Neprochnov, Y. P., and others, editors, Initial Reports of the Deep Sea Drilling Project, v. 42, Part 2: Washington, D. C., United States Government Printing Office, p. 737–748.
Irwin, H., Curtis, C., and Coleman, M., 1977, Isotopic evidence for source of diagenetic carbonates formed during burial of organic-rich sediments: Nature, v. 269, p. 209–213.
Jakobsen, R., and Postma, D., 1989, Formation and solid solution behavior of Ca-rhodochrosites in marine muds of the Baltic deeps: Geochimica et Cosmochimica Acta, v. 53, p. 2639–2648.
James, H. L., 1966, Chemistry of the iron-rich sedimentary rocks: United States Geological Survey Professional Paper 440-W, 61 p.
Klein, C., and Beukes, N. J., 1989, Geochemistry and sedimentology of a facies transition from limestone to iron-formation deposition in the early Proterozoic Transvaal Supergroup, South Africa: Economic Geology, v. 84, p. 1733–1774.
Koenings, J. P., 1976, In situ experiments on the dissolved and colloidal state of iron in an acid bog lake: Limnology and Oceanography, v. 21, p. 674–683.
Lee, R. W., 1985, Geochemistry of groundwater in Cretaceous sediments of the southeastern Coastal Plain, eastern Mississippi and western Alabama: Water Resources Research, v. 21, p. 1545–1556.
Lee, R. W., and Strickland, D. J., 1988, Geochemistry of groundwater in Tertiary and Cretaceous sediments of the southeastern Coastal Plain in Eastern Georgia, South Carolina, and southeastern North Carolina: Water Resources Research, v. 24, p. 291–303.
Leuchs, W., and Obermann, P., 1992, Anoxic reaction zones in an aquifer influenced by increasing nitrate and sulfate contents, *in* Matthess, G., Frimmel, F. H., Hirsch, P., Schulz, H. D., and Usdowski, E., editors, Progress in Hydro-Geochemistry: Berlin, Springer-Verlag, p. 201–212.
Matsumoto, R., and Iijima, A., 1981, Origin and diagenetic evolution of Ca-Mg-Fe carbonates in some coalfields of Japan: Sedimentology, v. 28, p. 239–259.
Mayer, L. M., and Gloss, S. P., 1980, Buffering of silica and phosphate in a turbid river: Limnology and Oceanography, v. 25, p. 12–22.
Maynard, J. B., 1982, Extension of Berner's "New Geochemical Classification of Sedimentary Environments" to ancient sediments: Journal of Sedimentary Petrology, v. 52, p. 1325–1331.
———— 1983, Geochemistry of Sedimentary Ore Deposits: New York, Springer-Verlag, 305 p.
McKnight, D. M., Kimball, B. A., and Bencala, K. E., 1988, Iron photoreduction and oxidation in an acidic mountain stream: Science, v. 240, p. 637–640.
Miles, C. J., and Brezonik, P. L., 1981, Oxygen consumption in humic-colored waters by a photochemical ferrous-ferric catalytic cycle: Environmental Science and Technology, v. 15, p. 1089–1095.

Moore, S. E., Ferrell, R. E., Jr., and Aharon, P., 1992, Diagenetic siderite and other ferroan carbonates in a modern subsiding marsh sequence: Journal of Sedimentary Petrology, v. 62, p. 357–366.

Morgan, J. J., and Stumm, 1964, Advances in water pollution research, *in* Proceedings of the Second Conference on Water Pollution Research: Elmsford, New York, Pergamon Press.

Morse, J. W., and Mackenzie, F. T., 1990, Geochemistry of Sedimentary Carbonates: New York, Elsevier Scientific Publications Company, 696 p.

Mozley, P. S., and Carothers, W. W., 1992, elemental and isotopic composition of siderite in the Kuparuk Formation, Alaska: Effect of microbial activity and water/sediment interaction on early pore-water chemistry: Journal of Sedimentary Petrology, v. 62, p. 681–692.

Mucci, A., 1988, Manganese uptake during calcite precipitation from seawater: Conditions leading to the formation of a pseudokutnahorite: Geochimica et Cosmochimica Acta, v. 52, p. 1859–1868.

Murray, J. W., Jannasch, H. W., Honjo, S., Anderson, R. F., Reeburg, W. S., Top, Z., Friederich, G. E., Codispoti, L. A., and Izdar, E., 1989, Unexpected changes in the oxic/anoxic interface in the Black Sea: Nature, v. 338, p. 411–413.

Nordstrom, D. K., Plummer, L. N., Langmuir, D., Busenberg, E., May, H. M., Jones, B. F., and Parkhurst, D. L., 1990, Revised chemical equilibrium data for major water-mineral reactions and their limitations, *in* Melchior, D. C., and Bassett, R. C., editors, Chemical Modeling of Aqueous Systems II: American Chemical Society, Symposium Series 416, Washington, D.C., p. 398–413.

Perdue, E. M., 1979, Solution thermochemistry of humic substances: Acid-base equilibria of river water humic substances, *in* Jenne, E. A., editor, Chemical Modeling in Aqueous Systems: Speciation, Sorption, Solubility, and Kinetics: American Chemical Society Symposium Series 93, Washington, D.C., American Chemical Society, p. 99–114.

Perdue, E. M., Beck, K. C., and Reuter, J. H., 1976, Organic complexes of iron and aluminium in natural waters: Nature, v. 260, p. 418–420.

Plummer, L. N., and Busenberg, E., 1982, The solubilities of calcite, aragonite and vaterite in CO_2-H_2O solutions between 0 and 90°C, and an evaluation of the aqueous model for the system $CaCO_3$-CO_2-H_2O: Geochimica et Cosmochimica Acta, v. 46, p. 1011–1040.

Postma, D., 1977, The occurrence and chemical composition of Recent Fe-rich mixed carbonates in a river bog: Journal of Sedimentary Petrology, v. 47, p. 1089–1098.

———— 1981, Formation of siderite and vivianite and the pore-water composition of a Recent bog sediment in Denmark: Chemical Geology, v. 31, p. 225–244.

———— 1982, Pyrite and siderite formation in brackish and freshwater swamp sediments: American Journal of Science, v. 282, p. 1151–1183.

Pye, K., Dickson, J. A. D., Schiavon, N., Coleman, M. L., and Cox, M., 1990, Formation of siderite-Mg-calcite-iron sulphide concretions in intertidal marsh and sandflat sediments, north Norfolk, England: Sedimentology, v. 37, p. 325–343.

Reuter, J. H., 1977, Importance of heavy metal-organic matter interactions in natural waters: Geochimica et Cosmochimica Acta, v. 41, p. 325–334.

Robie, R. A., Hemingway, B. S., and Fisher, J. R., 1979, Thermodynamic properties of minerals and related substances at 298.15 K and 1 Bar (10^2 Pascals) pressure and at higher temperatures: United States Geological Survey Bulletin 1452, 456 p.

Ross, D. A., 1978, Summary of results of Black Sea drilling, *in* Ross, D. A., and Neprochnov, Y. P., editors, Initial Reports of the Deep Sea Drilling Project, v. 42, Part 2: Washington, D.C., U.S. Govt. Printing Office, p. 1149–1177.

Scholten, R., 1974, Role of the Bosporus in the Black sea chemistry and sedimentation, *in* Degens, E. T., and Ross, D. A., editors, The Black Sea—Geology, Chemistry and Biology: American Association of Petroleum Geologists Memoir 20, p. 115–126.

Schrader, H. J., 1978, Quaternary through Neogene history of the Black Sea, deduced from the paleoecology of diatoms, silicoflagellates, ebridians and chrysomonads, *in* Ross, D. A., Neprochnov, Y. P., and others, editors, Initial Reports of the Deep Sea Drilling Project, v. 42, Part 2: Washington D.C., United States Government Printing Office, p. 789–901.

———— 1979, Quaternary paleoclimatology of the Black Sea basin: Sedimentary Geology, v. 23, p. 165–180.

Shapiro, J., 1964, Effect of yellow organic acids on iron and other metals in water: Journal of American Water Works Association, v. 56, p. 1062–1082.

Shatilova, I. I., Macharadze, N. V., and Davitashvili, L. S., 1991, The Pliocene climate of western Georgia, *in* Pliocene Climates of the Northern Hemisphere, Joint US/USSR Workshop on Pliocene Paleoclimates, Moscow, April, 1990, (Abstracts published by United States Geological Survey, Open-File Report, p. 35–37).

Shatilova, I. I., and Mchedlishvili, N. Sh., 1980, Palynological complexes of Chauda sediments of the West Georgia and their stratigraphic significance (in Russian): Tbilisi, Metsniereba, 96 p.

Shock, E. L., and Helgeson, H. C., 1988, Calculation of the thermodynamic and transport properties of aqeous species at high pressures and temperatures: Correlation algorithms for ion species and equation of state predictions to 5 kb and 1000°C; Geochimica et Cosmochimica Acta, v. 52, p. 2009–2036.

Sholkovitz, E. R., 1976, Flocculation of dissolved organic and inorganic matter: Geochimica et Cosmochimica Acta, v. 40, p. 831–845.

Sigurdsson, H., Devine, J. D., Tehoua, F. M., Presser, T. S., Pringle, M. K. W., and Evans, W. C., 1987, Origin of the lethal gas burst from Lake Monoun, Cameroun: Journal of Volcanology and Geothermeral Research, v. 31, p. 1–16.

Sirenko, N. A., and Turlo, S. I., 1986, Development of the Ukrainian soil and vegetation through the Pliocene and the Pleistocene: Kiev, Naukova Dumka, 180 p.

Smith, S. V., and Hollibaugh, J. T., 1993, Coastal metabolism and the oceanic organic carbon balance: Reviews of Geophysics, v. 31, p. 75–89.

Smith, S. V., and Mackenzie, F. T., 1987, The ocean as a net heterotrophic system: Implications from the carbon biogeochemical cycle: Global Biogeochemical Cycles, v. 1, p. 187–198.

Spell, T. L., and McDougall, I., 1992, Revisions to the age of the Brunhes-Matuyama boundary and the Pleistocene geomagnetic polarity time scale: Geophysical Research Letters, v. 19, p. 1181–1184.

Spiro, B., Gibson, P. J., and Shaw, H. F., 1993, Eogenetic siderites in lacustrine oil shales from Queensland, Australia, a stable isotope study: Chemical Geology, v. 106, p. 415–427.

Stoffers, P., and Müller, G., 1978, Mineralogy and lithofacies of Black Sea sediments, Leg 42, Part 2 Deep Sea Drilling Project, *in* Ross, D. A., Neprochnov, Y. P., and others, editors, Initial Reports of the Deep Sea Drilling Project, v. 42, Part 2: Washington, D. C., United States Government Printing Office, p. 1149–1177.

Suc, J. P., 1984, Origin and evolution of the Mediterranean vegetation and climate in Europe: Nature, v. 307, p. 429–432.

Sulzerber, B., Suter, D., Siffert, C., Banwart, S., and Stumm, W., 1989, Dissolution of Fe(III)(hydr)oxides in natural waters; laboratory assessment on the kinetics controlled by surface coordination: Marine Chemistry, v. 28, p. 127–144.

Suter, D., Siffert, C., Sulzerberger, B., and Stumm, W., 1988, Catalytic dissolution of Iron(III)(hydr)oxides by oxalic acid in the presence of Fe(II): Naturwissenschaften, v. 75, p. 571–573.

Tardy, Y., and Garrels, R. M., 1976, Prediction of Gibbs energies of formation—I. Relationships among Gibbs energies of formation of hydroxides, oxides, and aqueous ions: Geochemica et Cosmochemica Acta, v. 40, p. 1051–1056.

Theis, T. L., and Singer, P. C., 1973, The stabilization of ferrous iron by organic compounds in natural waters, *in* Singer, P. C., editor, Trace Metals and Metal-Organic Interactions in Natural Waters: Ann Arbor, Ann Arbor Science Publishers, p. 303–320.

———— 1974, Complexation of iron (II) by organic matter and its effect on iron (II) oxygenation: Environmental Science and Technology, v. 8, p. 569–573.

Thunell, R., Rio, D., Sprovieri, R., and Vergnaud-Grazzini, C., 1991, An overview of the post-Messinian paleoenvironmental history of the western Mediterranean: Paleoceanography, v. 6, p. 143–164.

Tipping, E., and Ohnstad, M., 1984, Colloid stability of iron oxide particles from a freshwater lake: Nature, v. 308, p. 266–268.

Traverse, A., 1978, Palynological analysis of DSDP Leg 42, Part 2 cores from the Black Sea, *in* Ross, D. A., Neprochnov, Y. P., and others, editors, Initial Reports of the Deep Sea Drilling Project, v. 42, Part 2: Washington, D.C., United States Government Printing Office, p. 993–1016.

Trendall, A. F., and Blockley, J. G., 1970, The iron formations of the Precambrian Hamersley Group, Western Australia: Geological Survey of Western Australia Bulletin 119, 366 p.

Ver, L. B., Mackenzie, F. T., and Lerman, A., 1994, Modeling pre-Industrial C-N-P-S biogeochemical cycling in the land-coastal margin system: Chemosphere, v. 29, p. 855–887.
Walker, J. C. G., 1984, Suboxic diagenesis in banded iron formations: Nature, v. 309, p. 340–342.
Walker, L. C., 1991, The Southern Forest: A chronicle: Austin, The University of Texas Press, 322 p.
Waite, T. D., and Morel, F. M. M., 1984, Photoreductive dissolution of colloidal iron oxides in natural waters: Environmental Science and Technology, v. 18, p. 860–868.
Warman, H. J., 1964, Alpha map transparencies mid-continental U.S.A.: Boston, Allyn and Bacon, 33 p.
Whiticar, M. J., Faber, E., and Schoell, M., 1986, Biogenic methane formation in marine and freshwater environments: CO_2 reduction vs. acetate formation-isotope evidence: Geochimica et Cosmochimica Acta, v. 50, p. 693–709.
Wollast, R., and Mackenzie, F. T., 1989, Global biogeochemical cycles and climate, *in* Berger, A., Schneider, S., and Duplessy, J., editors, Climate and Geo-Sciences: Dordrecht, Kluwer Academic Publishers, p. 453–473.
Wollast, R., Mackenzie, F. T., and Bricker, O. P., 1968, Experimental precipitation and genesis of sepiolite at earth-surface conditions: American Mineralogist, v. 53, p. 1645–1662.
Woods, T. L., and Garrels, R. M., 1992, Calculated aqueous-solution-solid-solution relations in the low temperature system CaO-MgO-FeO-CO_2-H_2O: Geochimica et Cosmochimica Acta, v. 56, p. 3031–3043.
Zubakov, V. A., and Borzenkova, I. I., 1990, Global Palaeoclimate of the Late Cenozoic: Amsterdam, Elsevier, 456 p.